

Copper–oxygen dynamics in tyrosinase

Nobutaka Fujieda,^{1,2*} Kyohei Umakoshi,¹ Yuta Ochi,² Yosuke Nishikawa,³ Sachiko Yanagisawa,⁴
Minoru Kubo,⁴ Genji Kurisu,³ & Shinobu Itoh^{1*}

¹Department of Material and Life Science, Graduate School of Engineering, Osaka University, 2-1 Yamada-oka, Suita, Osaka 565-0871, Japan

and

²Department of Applied Life Sciences, Graduate School of Life and Environmental Sciences, Osaka Prefecture University, 1-1 Gakuen-cho, Naka-ku, Sakai-shi, Osaka 599-8531, Japan

and

³Institute for Protein Research, Osaka University, 3-2 Yamada-oka, Suita, Osaka 565-0871, Japan

and

⁴Graduate School of Life Science, University of Hyogo, 3-2-1 Kouto, Kamigori-cho, Ako-gun, Hyogo 678-1297, Japan.

The dinuclear copper enzyme tyrosinase activates O_2 to form a $(\mu-\eta^2:\eta^2$ -peroxido)dicopper(II) species, which hydroxylates phenols to catechols. Although synthetic bis(μ -oxido)dicopper(III) complexes are observed as reactive intermediates, such species have not been identified in reactions catalysed by tyrosinase. We examined the behaviour of the copper-oxygen species in tyrosinase upon substrate-binding and updated the catalytic mechanism of tyrosinase. Here, we show the high-resolution X-ray crystal structures of the active forms, in which CuA is attracted to *L*-tyrosine (CuA1 \rightarrow CuA2), whose phenol oxygen directly coordinates to CuA2, involving the movement of CuB (CuB1 \rightarrow CuB2). The crystal structures and spectroscopic analyses of the dioxygen-bound forms demonstrated that the peroxide ligand rotated, spontaneously weakening its O–O bond. These results indicate that the copper migration induced by substrate-binding initiates the activation of the bound peroxide species and facilitates one of the peroxide oxygen atoms to access to the phenol substrate's ϵ carbon atom.

Direct oxidation of non-activated C–H bonds is still a great challenge in modern synthetic chemistry¹. In nature, monooxygenases catalyse various oxy-functionalization reactions under very mild conditions and have thus attracted broad interest as promising candidates for green catalysts². However, the catalytic mechanisms of non-haem iron or copper monooxygenases remain obscure relative to those of P450 haem monooxygenases³. Tyrosinases (EC 1.14.18.1) are ubiquitous dinuclear copper monooxygenases widely distributed in nature⁴. During the catalytic cycle, the copper centre is proposed to undergo three states—met-form ($(\mu\text{-hydroxido})\text{dicopper(II)}$ species, Fig. 1a, A), deoxy-form (reduced dicopper(I) species, Fig. 1a, B), and oxy-form ($(\mu\text{-}\eta^2\text{:}\eta^2\text{-peroxido})\text{dicopper(II)}$ species^{4–8}, Fig. 1a, C)—leading two successive reactions—hydroxylation of phenols to catechols (phenolase activity, Fig. 1a, C \rightarrow F) and oxidation of catechols to *o*-quinones (catecholase activity, Fig. 1a, A \rightarrow B)^{9–12}. The former hydroxylation reaction of phenol substrates by the oxy-form is the most attractive process among the chemical functions of tyrosinase from the viewpoint of dioxygen activation chemistry. In both synthetic modelling reactions and actual enzymatic systems, it has been proposed that the oxygenation of phenols by the $(\mu\text{-}\eta^2\text{:}\eta^2\text{-peroxido})\text{dicopper(II)}$ intermediate proceeds via electrophilic aromatic substitution reaction after the binding of deprotonated phenol, phenolate (Fig. 1a, C \rightarrow E)^{9,13–15}. On the other hand, in a model reaction, Stack et al. have demonstrated that the peroxide species is converted to an isomeric $\text{bis}(\mu\text{-oxido})\text{dicopper(III)}$ species when a phenolate substrate binds to the copper ion of the $(\mu\text{-}\eta^2\text{:}\eta^2\text{-peroxido})\text{dicopper(II)}$ species during the phenol-oxygenation reaction¹⁶. Nonetheless, there has been so far no report for the direct detection of such a $\text{bis}(\mu\text{-oxido})\text{dicopper(III)}$ species in the actual enzymatic reaction even at low temperatures¹⁷. In any case, the key step involves a coordinative interaction between the phenolate and copper ion in the catalytic cycle (Fig. 1a, C \rightarrow D). Here, we provide a novel insight into the catalytic mechanism of the dinuclear copper monooxygenase tyrosinase, including the rearrangement of copper-oxygen species as well as the intramolecular migration of the copper ion upon substrate-binding. Our results update the

information about the action mechanism of dinuclear copper enzymes during the catalytic reaction, replacing the previous model depicted by simple electrophilic aromatic substitution (Fig. 1a, C → E)^{9,13–15}.

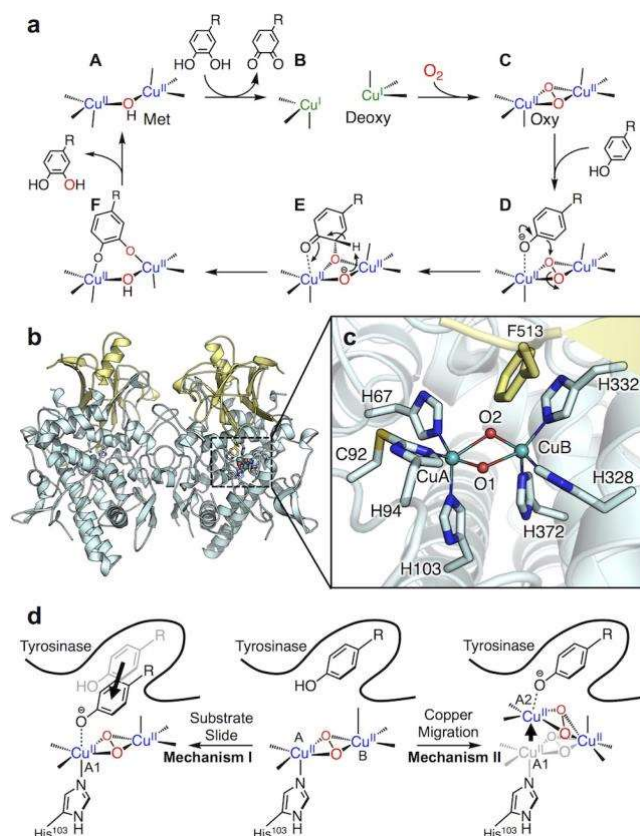


Figure 1 | Proposed tyrosinase catalytic cycle and crystal structure of the pro-form (inactive precursor) of the *Aspergillus* tyrosinase. **a**, Schematic representation of the catalytic cycle of tyrosinase. **b**, **c**, Overall homodimeric structure [chain A (left) and B (right)] (**b**) and dinuclear copper centre (met-form) of wild type tyrosinase (**c**) (PDB code: 3W6W). The copper-binding domain and C-terminal domain are indicated in blue and yellow, respectively. The protein main chains are displayed as ribbons, and the key amino acid residues are highlighted as sticks. **d**, Two mechanistic models for the step coordinating phenol substrate to the copper ion in the hydroxylation reaction.

Hydroxylation of pseudo-substrate

In the reported crystal structures of tyrosinases (Fig. 1b, c, and Extended Data Fig. 1)^{18–20}, the four-helix bundle core bears an anti-ferromagnetically coupled dinuclear copper centre, where each copper ion (called CuA and CuB, Fig. 1b, c, and Extended Data Fig.1) is linked by three histidine side chains (a His-X(n)-His-X(8)-His sequence for CuA and a His-X(3)-His-X(n)-His sequence for CuB, respectively)⁴. The pro-form of the *Streptomyces* tyrosinase is inactive because a subunit, so-

called caddie protein, shields the active site from the solvent. Interestingly, Tyr98 of the caddie protein is anchored into the pocket close to the copper-binding site as a “pseudo-substrate”, suggesting that this pocket is likely to be the substrate-binding site (Extended Data Fig. 1a and b)¹⁸. As the phenol oxygen atom (O ζ (Tyr98)) is relatively distant from the copper ion (CuA) (3.8 Å), it has been proposed that this pocket is the *pre*-substrate-binding site, and the bound phenol substrate slides toward CuA to make a direct coordinative interaction, initiating the hydroxylation reaction (Fig. 1d, Mechanism I, middle \rightarrow left)^{10,12,18,20}. However, such a substrate movement is impossible with the pseudo-substrate Tyr98 because its position is tightly fixed by the covalent linkage to the protein backbone. On the other hand, in the crystal structure of the Zn-substituted *Bacillus* tyrosinase containing L-tyrosine (Extended Data Fig. 1c and d), it has been found that the bound L-tyrosine occupied the same space as Tyr98 in *Streptomyces* tyrosinase, and ZnA is positioned near the phenolic oxygen, making a direct coordinative interaction (Extended Data Fig. 1d, e)²⁰. In this case, one of the metal ligands, His69, is detached from ZnA²⁰. Based on these observations, it has alternatively been proposed that this binding site is a true substrate-binding site but not the *pre*-substrate-binding site²⁰. More recently, it has been reported that incubation of *Streptomyces* tyrosinase crystal with a reductant under aerobic conditions leads to oxidation of Tyr98 of the caddie protein²¹. In this reaction, another electron density deriving from CuA appears (designated as CuA2), coordinated to the generated DOPA98 [2.3 Å, CuA2-O ζ (DOPA98)]²¹. Notably, the position of CuA2 is nearly the same as that of ZnA in the *Bacillus* tyrosinase, indicating that such an intramolecular migration of CuA may be necessary to induce the substrate hydroxylation reaction (Fig. 1d, Mechanism II, middle \rightarrow right)²¹. To conclude whether substrate sliding (Fig. 1d, mechanism I) or copper migration (Fig. 1d, Mechanism II) is the actual mechanism, atomic-level structural information about a Cu-bound tyrosinase containing L-tyrosine will be necessary.

We had previously reported a high-resolution crystal structure of the pro-form tyrosinase from *Aspergillus oryzae* (Fig. 1b, c)¹⁹. This form (pro-form) does not exhibit catalytic activity, because it includes the C-terminal domain, which shields the copper active site, and Phe513 of the C-

terminal domain is inserted into the substrate-binding site in the same way as Tyr98 of the caddie protein of the *Streptomyces* tyrosinase does (Fig. 1c and Extended Data Fig. 1d)^{18,19}. In this study, we initially prepared the pro-form of the copper-bound Phe513Tyr mutant (pro-F513Y, Extended Data Fig. 2) and determined its crystal structure (PDB code: 6JU4, Extended Data Fig. 3a-3d, Extended Data Tables 1, and Supplementary Table 2 and 3) to investigate the tyrosine-oxidation chemistry in the pro-form enzyme. In this case as well, the mutated Tyr513 residue was partially hydroxylated to DOPA513 (Extended Data Fig. 3c and Extended Data Tables 2) as found with the *Streptomyces* tyrosinase, where Tyr98 of the caddie protein was oxidized to DOPA, as mentioned above. Moreover, the two elongated electron densities at the CuA and CuB sites were observed, each of which could be assigned to two copper ions (CuA1 and CuA2, and CuB1 and CuB2, respectively; Extended Data Fig. 3d). This result suggested that the copper-binding sites of tyrosinases have the fluxional properties in common (see Supplementary Discussion).

To elucidate the dynamic behaviour of the copper ions and the binding mode of L-tyrosine (external phenolic substrates) during the catalytic cycle, an active-form of tyrosinase (ac-tyrosinase), whose *C*-terminal domain is truncated, was prepared by trypsin treatment according to the procedures we had previously reported²². However, all our efforts have failed so far because the ac-tyrosinase auto-oxidizes its tyrosine residues, leading to denaturation and aggregation even in the presence of tyrosinase inhibitors and/or metal chelators, such as EDTA and phenanthroline. Therefore, we used a hypomorphic Cys92Ala (C92A) mutant. In the *Aspergillus* tyrosinase, Cys92 is covalently bound to His94, one of the CuA-ligands, forming a His-Cys cross-link^{19,23}. This cross-linkage may contribute to the catalytic activity based on our previous enzymatic assay result but appears to be somewhat redundant for the catalytic activity (Extended Data Table 3, see Supplementary Discussion)²³. The C92A mutant exhibits lower activity toward L-tyrosine than the wild type (WT), but it still maintains a phenolase activity comparable to those of other tyrosinases with or without the His-Cys cross-link reported previously (Extended Data Table 3). In addition, in the crystal structure of the Cys92Ala/Phe513Tyr mutant (PDB code: 6JU5, pro-C92A/F513Y

without the His-Cys link), similar phenomena, including the self-hydroxylation of Tyr513 and copper migration, were also observed as is the case with pro-F513Y (Extended Data Fig. 3e, f, see Supplementary Discussion).

Detailed binding mode of L-Tyrosine

We succeeded to determine the crystal structures of four kinds of its derivatives, copper-depleted form with/without L-tyrosine [ac-C92A with L-tyrosine (ac-C92A-tyrosine (PDB code: 6JU7) and ac-C92A (PDB code: 6JU6)], and copper-containing form with/without L-tyrosine [ac-C92A-Cu-tyrosine (PDB code: 6JU9) and ac-C92A-Cu (PDB code: 6JU8)] at near-atomic resolutions of 1.42 Å, 1.50 Å, 1.42 Å, and 1.27 Å, respectively (Fig. 2 and Extended Data Figs. 4 and 5, Extended Data Table 1, and Supplementary Table 2). All these structures contain one pseudo-homodimeric structure (chain A and B) of the active-form of the C92A mutant without the C-terminal domain in a symmetric lattice (Extended Data Fig. 4, the whole detailed structure is described in Supplementary Discussion). In the pro-form, in the absence of copper ions (ac-C92A), water molecules (O2-4) exist in the place of Phe513, forming a hydrogen-bond network (Fig. 2b). Notably, the crystal structure of ac-C92A-tyrosine (without Cu) showed the clear electron density due to the bound L-tyrosine embedded in the substrate-binding site, which is occupied by Phe513 in the pro-form with high occupancies [77% (chain A) and 75 % (chain B), Fig. 2c and Extended Data Table 2]. This result strongly demonstrated that the binding mode of L-tyrosine was governed by the π - π interaction with His332, CH- π interaction with Val359, and hydrogen bond with Asn333 and Ser357 in the substrate-binding site (Fig. 2c), but not by the coordinative interaction of the phenolic oxygen with the copper ion. Importance of the interaction of CH- π with Val359 and the hydrogen bonding with Asn333 was confirmed by the L-tyrosine activity assay with the Val359Ala (V359A) and Asn333Ala (N333A) mutants. In these assays, the turnover numbers (k_{cat} values) were almost the same as that of WT, but the Michaelis constants (apparent dissociation constant of the substrate, K_m) drastically increased from 90 to 1.4×10^2 and 1.6×10^3 (μM), respectively (Extended

Data Table 3). Such weaker substrate-binding (larger K_m values) of the V359A and N333A mutants support the importance of the interaction of CH- π with Val359 and the hydrogen bonding with Asn333.

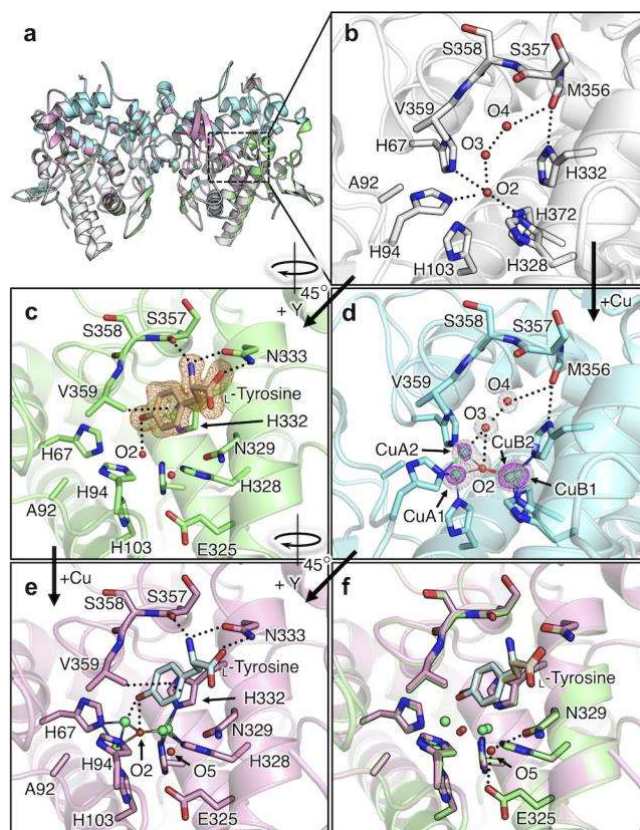


Figure 2 | Crystal structures of the active-form C92A mutant. **a**, Superimposed overall homodimeric structure [chain A(left) and B(right)] of the active-form C92A mutants [ac-C92A (white, PDB code: 6JU6), ac-C92A-tyrosine (green, PDB code: 6JU7), ac-C92A-Cu (blue, PDB code: 6JU8), and ac-C92A-Cu-tyrosine (pink, PDB code: 6JU9)]. **b-e**, The copper-binding sites of the active-form C92A mutants [ac-C92A (**b**), ac-C92A-tyrosine (**c**), ac-C92A-Cu (**d**), and ac-C92A-Cu-tyrosine (**e**)]. **f**, Superimposed structure of the substrate-binding sites of the tyrosine-bound active-form C92A mutants [ac-C92A-tyrosine (green) and ac-C92A-Cu-tyrosine (pink)]. The protein main chains are displayed as ribbons, and the key amino acid residues are highlighted as sticks. The $2Fo-Fc$, omit ($Fo-Fc$), and anomalous maps are contoured at 1.5, 4.0, and 5.0 σ , and shown in gray, orange, and magenta mesh, respectively.

Copper migration upon substrate-binding

Interestingly, the crystal structure of the copper-bound C92A mutant (C92A–Cu without tyrosine) at a near-atomic resolution showed two clear anomalous peaks around the CuA site corresponding to CuA1 and CuA2 even in the absence of coordinating substrates such as tyrosine (Fig. 2d). CuA2 supported by His67 and His94 remained in its place but shifted away from the CuA1 position supported by His67, His94, and His103 by 2.11 Å (in chain A) and 2.09 Å (in chain B), and its occupancy was 29% in chain A and 23 % in chain B (CuA1, 51% and 59% in chains A and B, respectively). Furthermore, at the CuB site, another elongated anomalous electron density was observed, which can be assigned to two copper ion positions (CuB1 and CuB2; Fig. 2d). CuB2 was supported by the three histidine residues (His328, His332, and His372) and located at the same position as CuB in pro-WT, while CuB1 was placed away from CuB2 by 0.62 Å (in chain A) and 0.72 Å (in chain B), being closer to His332 and His372. Occupancies of CuB1 and CuB2 were determined to be 53 % and 40 % in chain A, and 60 % and 30 % in chain B, respectively (Extended Data Table 2). Even in the presence of copper ions, water molecules (O2-4) were present in the places of the Phe513 residues (Extended Data Fig. 2d). Water molecule O3, in particular, coordinated to CuA2 with a distance of 2.22 Å (in chain A) and 2.34 Å (in chain B), and perturbed the equilibrium between CuA1 and CuA2 (Fig. 2d). Thus, the near-atomic resolution crystal structure unveiled the detailed copper positions in the active-form of tyrosinase (ac-C92A).

Notably, ac-C92A–Cu–tyrosine (the enzyme–copper–substrate ternary complex) also exhibited the clear electron density deriving from the bound *L*-tyrosine in the same position as in the crystal of ac-C92A–tyrosine (without copper), demonstrating the identical substrate-binding mode (Fig. 2e and f, and Extended Data Fig. 5a-d). In comparison with Tyr513 in the pro-form, however, the phenol moiety significantly rotated by 30° toward CuA2 (Extended Data Fig. 5e and f), providing more accurate information about coordination geometry in the substrate complex than that of pseudo-substrate (Hydroxylation of the bound tyrosine is described in Supplementary Discussion). The phenol oxygen atom of the bound-*L*-tyrosine apparently coordinated to CuA2

(2.01 Å in chain A and 2.19 Å in chain B), and the occupancies of CuA2 clearly increased compared with those in ac-C92A–Cu without the L-tyrosine (29 % → 37 % in chain A and 23 % → 26 % in chain B). Thus, substrate-binding perturbed the copper position, indicating that the hydroxylation reaction was triggered by such copper migration (CuA1 → CuA2, Fig 1d, Mechanism II) rather than the position shift of the substrate (Fig 1d, Mechanism I). If this is the case, it is possible that His103 detached from the copper ion and acted as a base to accept a proton from the phenol substrate, enhancing the substrate's coordination to CuA2, although a water molecule (O5, Fig. 2f) activated by the conserved amino acid residues (glutamate and asparagine) has been proposed to act as a base to de-protonate the phenol substrates^{20,24}. On the other hand, the occupancies of CuB2 were also clearly increased compared with those in ac-C92A–Cu (40 % → 43 % in chain A and 30 % → 42 % in chain B), indicating that substrate-binding caused the rearrangement of the dinuclear copper centre, CuB site (CuB1 → CuB2) as well as CuA site (CuA1 → CuA2). The distances between CuA2 and CuB2 (3.33 Å in chain A and 3.35 Å in chain B) were found to be much shorter than those between CuA1 and CuB1 (4.17 Å in chain A and 4.24 Å in chain B). This observation clearly demonstrates that substrate-binding makes the CuA–CuB distance closer to that of the (μ - η^2 : η^2 -peroxido)dicopper(II) complexes (\sim 3.5 Å)^{5,6,25}.

Activation of copper-oxygen species

For further insight into the significance of such an intramolecular migration of copper ions in the catalytic cycle, we scrutinized the differences between the oxy-forms of the pro-C92A and pro-C92A/H103F mutants by crystal structure analysis as well as UV-vis and resonance Raman spectroscopic analyses. The pro-C92A mutant was employed to retain the CuA1 state (His103-coordinating form), and the pro-C92A/H103F mutant was prepared to mimic the CuA2 state (His103-detaching form). We had previously reported that the copper-depleted form of pro-C92A was converted into the oxy-form upon the addition of CuSO₄, which is stable due to the blocking of the substrate's access to the dioxygen-binding site by Phe513 as the substrate-analog²³. The pro-

C92A/H103F mutant can also stabilize the oxy-form to give a characteristic UV-visible absorption spectrum exhibiting an intense LMCT band at $\lambda_{\max} = 332$ nm ($\epsilon = 1.2 \times 10^4$ M⁻¹ cm⁻¹) and a weak LMCT band at 568 nm (5.1×10^2 M⁻¹ cm⁻¹) due to the (μ - η^2 : η^2 -peroxido)dicopper(II) intermediate (Fig. 3a). In the Raman spectrum, there were three isotope-sensitive signals assignable to the symmetric O–O vibration [$\nu_s(\text{O–O})$], and the fundamental and overtone of asymmetric Cu–O vibrations [$\nu_{\text{as}}(\text{Cu–O})$] of the (μ - η^2 : η^2 -peroxido)dicopper(II) core, observed at 737 cm⁻¹, 561 cm⁻¹, and 1123 cm⁻¹, respectively, which shifted to 704 cm⁻¹, 535 and 1069 cm⁻¹ upon ¹⁸O₂-substitution (Fig. 3b)²⁶. The $\nu_s(\text{O–O})$ signal shifted to lower energy (by 8 cm⁻¹) than that of pro-C92A-Cu (745 cm⁻¹), clearly indicating that the O–O bond was weakened²³.

We resolved the single crystal structures of pro-C92A–Cu (PDB code: 6JUB) and pro-C92A/H103F–Cu (PDB code: 6JUD, Extended Data Table 1, and Supplementary Table 2), but they did not have a clear electron density corresponding to the peroxide moiety between CuA and CuB, presumably because of the photo-reduction by X-ray irradiation (Extended Data Fig. 6a and b). To obtain a minimum-damaged crystal structure, we merged 18 crystal data in low X-ray dose and determined the structures of pro-C92A–Cu (PDB code: 6JUA) and pro-C92A/H103F–Cu (PDB code: 6JUC) at the resolutions of 1.45 Å and 1.44 Å, respectively, (Fig. 3c and d, Extended Data Fig. 6, Extended Data Table 1 and 2, and Supplementary Table 2). Although both crystallographic asymmetric units contained one homodimeric structure, the electron density of the peroxide species was observed only in chain B with high occupancies [72% (pro-C92A–Cu) and 82 % (pro-C92A/H103F–Cu), (Extended Data Fig. 6, Extended Data Table 2, see Supplementary Discussion)]. The oxy-form of pro-C92A–Cu involved a (μ - η^2 : η^2 -peroxido)dicopper(II) species with a slightly butterfly-bending structure (Fig. 3c, red stick and ball), whereas the oxy-form of pro-C92A/H103F–Cu showed a planer Cu₂O₂ core structure (Fig. 3d, yellow stick and ball). CuB is located at the CuB2 position in both structures. On the other hand, CuA occupies the CuA1 and CuA2 positions in the oxy-forms of pro-C92A and pro-C92A/H103F, respectively, as we expected

(Extended Data Fig. 6f, the detailed coordination geometry is described in Supplementary Discussion).

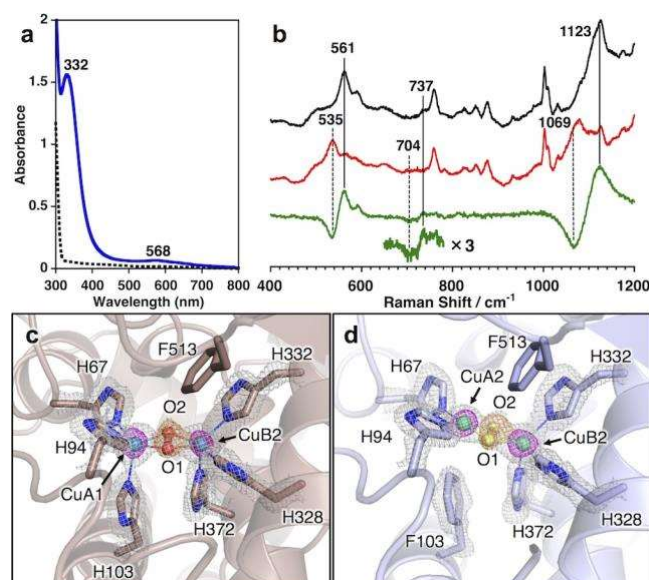


Figure 3 | Spectroscopic analyses and crystal structures of two oxy-form C92A mutants. **a**, UV-vis spectra of pro-C92A/H103F-Cu (blue) and copper-depleted pro-C92A/H103F (dotted black) **b**, Resonance Raman spectra of the oxy-form of C92A/H103F (black, with $^{16}\text{O}_2$; red, with $^{18}\text{O}_2$; green, differential spectrum between the above two spectra) **c**, **d**, The structures of the dinuclear copper centres with the peroxide of pro-C92A-Cu (Chain B, PDB code: 6JUA) (**c**) and pro-C92A/H103-Cu (Chain B, PDB code: 6JUC) (**d**). The protein main chains are displayed as ribbons, and the key amino acid residues are highlighted as sticks. The $2F_o - F_c$, omit ($F_o - F_c$), and anomalous maps are contoured at 1.8, 5.0, and 5.0 σ and shown in gray, orange, and magenta mesh, respectively.

The CuA-CuB and O-O bond distances in pro-C92A-Cu (Chain B) were determined to be $3.55 \pm 0.01 \text{ \AA}$ and $1.47 \pm 0.06 \text{ \AA}$, respectively (this O-O bond distance is compared with that of another tyrosinase in Supplementary Discussion). On the other hand, pro-C92A/H103F-Cu (Chain B) showed a shortened CuA-CuB bond distance by 0.07 \AA ($3.48 \pm 0.02 \text{ \AA}$) and an unusually elongated O-O bond distance by 0.07 \AA ($1.54 \pm 0.06 \text{ \AA}$). Although this O-O bond length is unusually long for (μ - η^2 : η^2 -peroxido)dicopper(II) species in a dinuclear copper protein, the length of $1.540 \pm 0.005 \text{ \AA}$ has been reported in the model compounds²⁷. These results clearly demonstrated that the intramolecular migration of the copper ion from the CuA1 position to the CuA2 position weakened the O-O bond of the peroxide ligand, causing enhancement of the reactivity of the peroxide intermediate at the CuA2-CuB2 position. This geometric structural change is significantly

reminiscent of the conversion of (μ - η^2 : η^2 -peroxido)dicopper(II) complex to bis(μ -oxido)dicopper(III) complex upon phenolate-binding in a model system¹⁶. Since there is no such phenolate ligand in pro-C92A/H103F-Cu, the Cu₂O₂ core still shows typical features of (μ - η^2 : η^2 -peroxido)dicopper(II) species. However, the substrate (tyrosinate) binding would provoke such a geometric change into the bis(μ -oxido)dicopper(III) species in the actual catalytic cycle.

Discussion

In the superimposed structure of pro-C92A-Cu (chain B), pro-C92A/H103F-Cu (chain B), and ac-C92A-Cu-tyrosine (chain B), the peroxide ligand rotates by 20° to approach to the ortho position (C ϵ atom) of the bound-L-tyrosine substrate, and axial ligands of CuA changed from His103 to L-tyrosine (distances of phenol oxygen to CuA2, 2.4 Å) by the intramolecular migration of CuA from A1 to A2 position (distances of O1 of the peroxide ion to C ϵ of L-tyrosine: 3.8 → 3.3 Å, Fig. 4a and b). To date, it has been proposed that the peroxide rotates by 90° after the substrate shift (Fig 1d, Mechanism I) induced by direct coordination of the phenolate oxygen to CuA1¹⁰. This allows the peroxide σ^* orbital to overlap with the π orbital of the phenolate C ϵ atom for the electrophilic attack of the peroxide to the aromatic ring of the substrate¹⁰. Our results are partially consistent with this proposal, but we have revealed that the peroxide rotation is induced not by the substrate slide but by the copper migration with the activation of O-O bond to facilitate the hydroxylation reaction. Such a peculiar geometrical change occurs even in the absence of the coordination of the bound-L-tyrosine to CuA2. In the superimposed structure, the distance between CuA1 in pro-C92A-Cu and CuA2 in pro-C92A/H103F-Cu (~1.5 Å) is shorter than that in ac-C92A-Cu-tyrosine (~2.0 Å). This means that the bound-L-tyrosine could substantially give rise to the copper migration, leading to more drastic geometrical changes, including peroxide rotation and O-O bond activation.

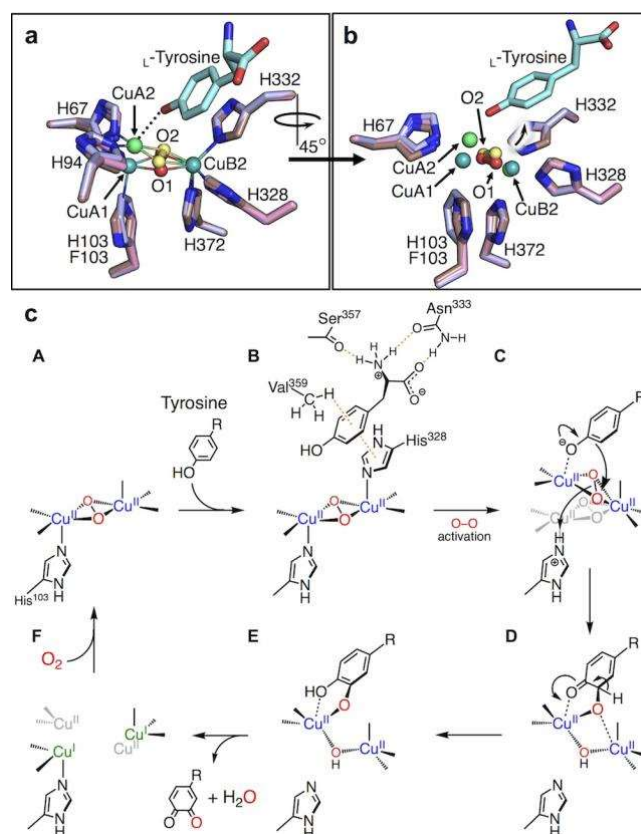


Figure 4 | Schematic representation of the proposed mechanism. **a, b**, Superimposed structure of the substrate binding site of pro-C92A–Cu (chain B, brown), pro-C92A/H103F–Cu (chain B, purple), and ac-C92A–Cu–tyrosine (chain B, pink). The protein main chains are displayed as ribbons, and the key amino acid residues are highlighted as sticks. **c**, Plausible catalytic cycle of tyrosinase.

Our updated mechanistic model is shown in Fig. 4 c. The tyrosine substrate binds to the restricted substrate-binding site through multiple non-covalent interactions with the amino acids (His332, Asn333, Ser357, and Val359; Fig. 4c, A → B). This substrate binding induces migration of CuA from the CuA1 position to the CuA2 position, approaching to the phenol moiety of the substrate. During this CuA migration, His103 is detached from the copper ion (Fig. 4c, B → C) providing a free base to accept a proton from the bound tyrosine substrate. Then, the generated tyrosinate (phenolate form) directly coordinates to the migrated CuA2 to induce O–O bond activation of the Cu₂O₂ core (possibly by converting the (μ - η^2 : η^2 -peroxido)dicopper(II) species to a bis(μ -oxido)dicopper(III)). The geometric change also induces rotation of the Cu₂O₂ plane so that one of the oxygen atoms can approach to the ortho-carbon of phenolate substrate, enhancing the

electrophilic attack to the substrate (Fig. 4c, C → D → E). After the oxidation of catechol to *o*-quinone via intramolecular electron-transfer, the CuA and CuB ions return to the CuA1 and CuB1 sites, respectively, thereby promoting dissociation of the product (Fig. 4c, E → F → A). Thus, the intramolecular copper migration drives efficient catalytic action of tyrosinases. The geometric transformation of copper–active oxygen species presented here is vastly different than that in other copper enzymes²⁸. Therefore, this work lays the foundation for the generation of a wide range of more efficient, robust, and useful catalysts in future while shedding light on the action mechanisms of other non-haem metalloenzymes.

Online Content Any methods, additional references, extended data, supplementary information, acknowledgements, details of author contributions, and competing interests, and code availability can be found at <https://doi.org/XXXXXXX>

1. Que, L. & Tolman, W. B. Biologically inspired oxidation catalysis. *Nature* **455**, 333–340 (2008).
2. Lewis, J. C., Coelho, P. S. & Arnold, F. H. Enzymatic functionalization of carbon–hydrogen bonds. *Chem. Soc. Rev.* **40**, 2003–2021 (2011).
3. Bordeaux, M., Galarneau, A. & Drone, J. Catalytic, mild, and selective oxyfunctionalization of linear alkanes: Current challenges. *Angew. Chemie Int. Ed.* **51**, 10712–10723 (2012).
4. Solomon, E. I. *et al.* Copper active sites in biology. *Chem. Rev.* **114**, 3659–853 (2014).
5. Mirica, L. M., Ottenwaelder, X. & Stack, T. D. P. Structure and spectroscopy of copper-dioxygen complexes. *Chem. Rev.* **104**, 1013–45 (2004).
6. Lewis, E. A. & Tolman, W. B. Reactivity of dioxygen-copper systems. *Chem. Rev.* **104**, 1047–76 (2004).
7. Keown, W., Gary, J. B. & Stack, T. D. P. High-valent copper in biomimetic and biological oxidations. *J. Biol. Inorg. Chem.* **22**, 289–305 (2017).
8. Quist, D. A., Diaz, D. E., Liu, J. J. & Karlin, K. D. Activation of dioxygen by copper metalloproteins and insights from model complexes. *J. Biol. Inorg. Chem.* **22**, 253–288 (2017).
9. Itoh, S. & Fukuzumi, S. Monooxygenase activity of type 3 copper proteins. *Acc. Chem. Res.* **40**, 592–600 (2007).
10. Rolff, M., Schottenheim, J., Decker, H. & Tucek, F. Copper-O₂ reactivity of tyrosinase models towards external monophenolic substrates: molecular mechanism and comparison with the enzyme. *Chem. Soc. Rev.* **40**, 4077–4098 (2011).
11. Kanteev, M., Goldfeder, M. & Fishman, A. Structure-function correlations in tyrosinases. *Protein Sci.* **24**, 1360–1369 (2015).
12. Hamann, J. N., Herzigkeit, B., Jurgeleit, R. & Tucek, F. Small-molecule models of tyrosinase: From ligand hydroxylation to catalytic monooxygenation of external substrates. *Coord. Chem. Rev.* **334**, 54–66 (2017).

13. Yamazaki, S. & Itoh, S. Kinetic evaluation of phenolase activity of tyrosinase using simplified catalytic reaction system. *J. Am. Chem. Soc.* **125**, 13034–13035 (2003).
14. Itoh, S. *et al.* Oxygenation of phenols to catechols by a (μ - η^2 : η^2 -peroxo)dicopper(II) complex: Mechanistic insight into the phenolase activity of tyrosinase. *J. Am. Chem. Soc.* **123**, 6708–6709 (2001).
15. Fujieda, N. & Itoh, S. Controlling dicopper protein functions. *Bull. Chem. Soc. Jpn.* **89**, 733–742 (2016).
16. Mirica, L. M. Tyrosinase reactivity in a model complex: An alternative hydroxylation mechanism. *Science* **308**, 1890–1892 (2005).
17. Spada, A., Palavicini, S., Monzani, E., Bubacco, L. & Casella, L. Trapping tyrosinase key active intermediate under turnover. *Dalt. Trans.* 6468-6471 (2009).
18. Matoba, Y., Kumagai, T., Yamamoto, A., Yoshitsu, H. & Sugiyama, M. Crystallographic evidence that the dinuclear copper center of tyrosinase is flexible during catalysis. *J. Biol. Chem.* **281**, 8981–90 (2006).
19. Fujieda, N. *et al.* Crystal structures of copper-depleted and copper-bound fungal pro-tyrosinase: insights into endogenous cysteine-dependent copper incorporation. *J. Biol. Chem.* **288**, 22128–22140 (2013).
20. Goldfeder, M., Kanteev, M., Isaschar-Ovdat, S., Adir, N. & Fishman, A. Determination of tyrosinase substrate-binding modes reveals mechanistic differences between type-3 copper proteins. *Nat. Commun.* **5**, 4505 (2014).
21. Matoba, Y. *et al.* Catalytic mechanism of the tyrosinase reaction toward the Tyr98 residue in the caddie protein. *PLOS Biol.* **16**, e3000077 (2018).
22. Fujieda, N. *et al.* Multifunctions of *MelB*, a fungal tyrosinase from *Aspergillus oryzae*. *Chembiochem* **13**, 193–201 (2012).
23. Fujieda, N. *et al.* Post-translational His-Cys cross-linkage formation in tyrosinase induced by copper(II)-peroxo species. *J. Am. Chem. Soc.* **133**, 1180–1183 (2011).

24. Solem, E., Tuzcek, F. & Decker, H. Tyrosinase versus catechol oxidase: One asparagine makes the difference. *Angew. Chemie Int. Ed.* **55**, 2884–2888 (2016).
25. Kitajima, N., Fujisawa, K., Morooka, Y. & Toriumi, K. μ - η^2 : η^2 -Peroxo binuclear copper complex, [Cu(HB(3,5-iPr₂pz)₃)₂(O₂)]. *J. Am. Chem. Soc.* **111**, 8975–8976 (1989).
26. Ling, J. *et al.* Common oxygen binding site in hemocyanins from arthropods and mollusks. Evidence from Raman spectroscopy and normal coordinate analysis. *J. Am. Chem. Soc.* **116**, 7682–7691 (1994).
27. Park, G. Y. *et al.* Geometric and electronic structure of [$\{\text{Cu}(\text{MeAN})\}_2(\mu$ - η^2 : η^2 (O₂²⁻))] ²⁺ with an unusually long O–O bond: O–O Bond weakening vs activation for reductive cleavage. *J. Am. Chem. Soc.* **134**, 8513–8524 (2012).
28. Shin, D. S. *et al.* Superoxide dismutase from the eukaryotic thermophile *Alvinella pompejana*: Structures, stability, mechanism, and insights into amyotrophic lateral sclerosis. *J. Mol. Biol.* **385**, 1534–1555 (2009).

METHODS

Chemicals. All the chemicals used were of the highest grade available and purchased from Sigma-Aldrich. $^{18}\text{O}_2$ was obtained from TAIYO NIPPON SANSO.

Preparation of proteins. Oligonucleotide-directed mutagenesis was performed on pETH-melB vector that contained the *melB* genomic DNA encoding the *Aspergillus* tyrosinase (wild type and C92A mutant)^{22,23}. The pair of approximately 25 nucleotide long mutagenic oligonucleotides (Supplementary Table 1) was purchased from Macrogen Japan Co. The site-directed mutagenesis was carried out by inverse PCR, followed by DpnI digestion and self-ligation. For the mutant, the absence of undesired mutations on the gene was confirmed by DNA sequencing using 3730xl DNA Analyzer (Applied Biosystems) after the construction of the vector. The pro-forms of the *Aspergillus* tyrosinases (F513Y, N333A, and V359A variants) were prepared in the copper-bound state by using pETH-melB plasmid as previously described^{22,23}. The series of mutants containing C92A mutation were prepared in the copper-depleted form as previously described^{22,23}. For purification of the C-terminal truncated wild type tyrosinases (active-form, ac-tyrosinase), we performed the activation procedure that we have reported previously²². We reoptimized the incubation time (1 h) and temperature (4 °C) of trypsin treatment for the purification of ac-C92A mutant. The pro-form tyrosinase purified as described previously was concentrated to 100 μM and mixed with the same volume of 1-mg/mL trypsin solution to excise the C-terminal domain. The reaction mixture was kept at 4 °C for 1 h and then the resulting sample was diluted with 10 mM Tris-HCl buffer (pH 8.7) by 50-fold. The diluted solution was loaded onto Q sepharose HP columns (5 ml, GE Healthcare), and then eluted with a linear gradient of NaCl (10-200 mM) in 10 mM Tris-HCl buffer (pH 8.7). The fractions containing the ac-tyrosinase were collected and concentrated by ultrafiltration using Vivaspin turbo 15. The protein samples were stored at -80 °C until use. Purity was determined by SDS-PAGE (Extended Data Fig. 2).

Crystallization of pro-tyrosinases. The purified protein solutions of the pro-form tyrosinases [copper-bound F513Y variant and copper-depleted C92A, C92A/H103F, and C92A/F513Y variants (pro-F513Y–Cu, pro-C92A, pro-C92A/H103F, and pro-C92A/F513Y, respectively)] were desalted using PD-10 columns (GE Healthcare) and changed to 5 mM Bis-tris buffer (pH 7.2). The protein solutions were concentrated and stored at –80 °C. Crystallization was performed by the hanging drop vapour diffusion method as previously described¹⁹. The reservoir solution (150 µl) containing 18% polyethylene glycol (PEG) 3350 and 30 mM NH₄NO₃ was added to a well of the crystallization plate. A drop of the precipitant solution containing 18% PEG 3350, 30 mM NH₄NO₃ (1 µL), and 16 mg/mL pro-tyrosinase solution (2 µL) was placed on a glass slide, which was subsequently placed on the well. The plate was placed in an incubator at 20 °C. After 1 day, the pro-C92A crystals were obtained. To obtain copper-bound pro-tyrosinase crystals, each pro-C92A, pro-C92A/H103F, and pro-C92A/F513Y crystal sample was soaked in 2-mM CuSO₄-containing preservative solution (20% PEG 3350, 30 mM NH₄NO₃, and 5 mM Bis-tris pH 7.2).

Crystallization of C-terminal truncated tyrosinases. The purified protein solution of the C-terminal truncated C92A [the copper-depleted form of active C92A (ac-C92A)] was desalted using PD-10 columns (GE Healthcare) and changed to 10-mM Tris-HCl buffer (pH 8.0). The protein solution was concentrated and stored at –80 °C. Crystallization was performed by the hanging drop vapour diffusion method. The reservoir solution (150 µL) containing 20% PEG 3350 and 30 mM NH₄NO₃ was added to a well of the crystallization plate. A drop of the precipitant solution containing 20% PEG 3350, 30 mM NH₄NO₃ (1 µL) and 10 mg/mL ac-C92A solution (2 µL) was placed on a glass slide, which was subsequently placed on the well. The plate was placed in an incubator at 20 °C. In 2 days, the ac-C92A crystals were obtained. To obtain copper-bound ac-C92A crystals (ac-C92A–Cu), ac-C92A crystal samples were soaked for 36 h in 0.10-mM CuSO₄-containing preservative solution (20% PEG 3350, 30 mM NH₄NO₃, and 5 mM Bis-tris pH 7.2). For the preparation of the substrate-tyrosinase binary complex (ac-C92A–tyrosine), ac-C92A

crystal samples were soaked in saturated L-tyrosine-containing preservative solution for 30 min. In the case of the substrate-copper-tyrosinase ternary complex (ac-C92A–Cu–tyrosine), copper solution-soaked crystals were subsequently soaked again in saturated L-tyrosine-containing preservative solution for 1 min.

X-ray data collection and structure determination. All the diffraction data were collected at the SPring-8 synchrotron facility (BL44XU, Harima, Hyogo, Japan). X-ray diffraction images were collected using MX300HE CCD detectors equipped with a cryo-system at 100 K using a wavelength of 0.90000 Å. Before flash cooling, crystals were soaked in a cryoprotectant solution (45 % PEG 3350, 30 mM NH₄NO₃, and 5 mM Bis-tris pH 7.2). The data were processed and scaled with the HKL-2000 program package. In the oxy-form of tyrosinase (pro-C92A–Cu and pro-C92A/H103F–Cu), the X-ray data were collected and merged with 18 isomorphous crystals to make a single minimum-damaged dataset using initially irradiated frames only. The data collection and refinement statistics are summarized in Extended Data Table 1. The crystal structures of the pro-forms were solved by molecular replacement with the Phaser program using the reported coordinate [wild type pro-tyrosinase (PDB code: 3W6W, chain A)] as a search model. Regarding the active-forms, the coordinate of the copper-binding domain in [PDB code: 3W6W, Pro1-Lys457(chain A)] was solely used instead of the whole coordinate. After the determination of the first structure, all following data sets of the ac-tyrosinase were resolved by molecular replacement using the apo-form structure (ac-C92A). The structure models were refined by the program phenix.refine²⁹, manually rebuilding with the program Coot³⁰. This procedure was iterated until the model did not further improve. Then, the structure model was further refined by SHELXL software (version 2017/1), manually rebuilding with Coot. At this stage, anisotropic temperature factors were adapted to all the atoms except water molecules and calculated with RIGU and SIMU instructions³¹. The restraint parameters of DFIX, DANG, and FLAT instructions for the substrate-bound L-tyrosine, L-DOPA, DOPA513 residue, and nitrate ion were generated by using Grade Web

Server (Global Phasing Ltd.). A subset of 5% of the reflections was separated to monitor the free R factor (R_{free}). In all the crystal structures, most of the residues were well defined in the final electron density, except for some disordered loops and amino acid residues in the flexible regions (Supplementary Table 2). The distances and angles among the copper ions and their ligand atoms including the peroxide ion were completely unrestrained during structure refinement because the resolution and the data-to-parameter ratio were high enough. The bond lengths and angles of the metal-coordinating atoms to each metal (for example, Cu–O and Cu-imidazole N ϵ distances) are summarized in Supplementary Table 2. The occupancies of copper ions, tyrosines (including Tyr513 residues), and peroxide ion (PER) are listed in Extended Data Table 2. In the structures, Ramachandran analysis with the Molprobity program showed no outliers³². The atomic coordinates of the final models and experimental structure factors have been deposited to the worldwide PDB and are accessible under the code described in Extended Data Table 1. Secondary structures were assigned by the DSSP program³³ and all the figures of the protein structures were prepared using PyMOL (version 1.8, Schrödinger LLC). The omit maps were calculated for the bound substrate (L-tyrosine and peroxide) and the O ϵ atom of DOPA513 residue. In superimposed structures, two or three protein molecules were aligned at C α atoms of six coordinating histidines.

Preparation of copper-bound pro-tyrosinases in solution. Purified pro-C92A/H103F solutions were loaded on PD-10 columns (GE Healthcare) pre-equilibrated with 50 mM potassium phosphate buffer (pH 7.2). The loaded sample was then eluted by the same buffer solution. Pro-tyrosinases (100 μ M) were treated with the same volume of CuSO₄ solution (200 μ M). The sample was incubated at 4 °C for 3 h and concentrated and desalted by ultrafiltration using Vivaspin turbo 15 to remove excess CuSO₄.

Activity assays. Trypsin (50 μ L of 1 mg/mL) was added to the purified copper-bound pro-tyrosinase samples in 10-mM Tris-HCl buffer (pH 8.2, 50 μ L). The mixture was stored at 4 °C for

30 min. The reaction was initiated by adding the trypsin-treated tyrosinase (2 μL) to L-tyrosine in 50 mM potassium phosphate buffer (2 mL total volume, pH 7.0) in a UV cell (1.0 cm path length). The reaction progress was followed by monitoring the increase in the absorbance at 475 nm ($\epsilon_{475} = 3600 \text{ M}^{-1}\text{cm}^{-1}$)³⁴ resulting from dopachrome by using an 8453 photodiode-array spectrophotometer (Agilent Technologies) maintained at 25 °C with a Peltier-controlled thermostated cell holder. Steady-state kinetic parameters [turnover number (k_{cat}) and Michaelis constant (K_{m})] were determined by nonlinear curve fitting of Michaelis–Menten plots [V_{obs} vs. (substrate)] from three measurements.

UV-vis and Resonance Raman Spectroscopy. UV-vis spectra measurements were performed using a UV-650 spectrophotometer (JASCO Co.). Resonance Raman spectra excited at 355 nm by using a sealed microchip laser SNV-20F (Teem Photonics) were measured with a 0.75-m single monochromator (SPEX, 750M) equipped with a liquid nitrogen-cooled CCD detector (Roper Scientific, PyLoN:400B-UV-HK). To prevent photo-damage to the samples, the sample cell was rotated at 1000 rpm, and the laser power at the sample point was set at 5 mW. A 90° light collection geometry was used.

Data availability

Structural models and factors have been deposited in the Protein Data Bank under the accession numbers 6JU4 (Pro-F513Y), 6JU5 (Pro-C92A/F513Y), 6JU6 (Ac-C92A), 6JU7 (Ac-C92A–tyrosine), 6JU8 (Ac-C92A–Cu), 6JU9 (Ac-C92A–Cu–tyrosine), 6JUA [Pro-C92A (oxy)], 6JUB [Pro-C92A (damaged)], 6JUC [Pro-C92A/H103F (oxy)], and 6JUD [Pro-C92A/H103F (damaged)].

29. Adams, P. D. *et al.* PHENIX : a comprehensive Python-based system for macromolecular structure solution. *Acta Crystallogr. Sect. D Biol. Crystallogr.* **66**, 213–221 (2010).

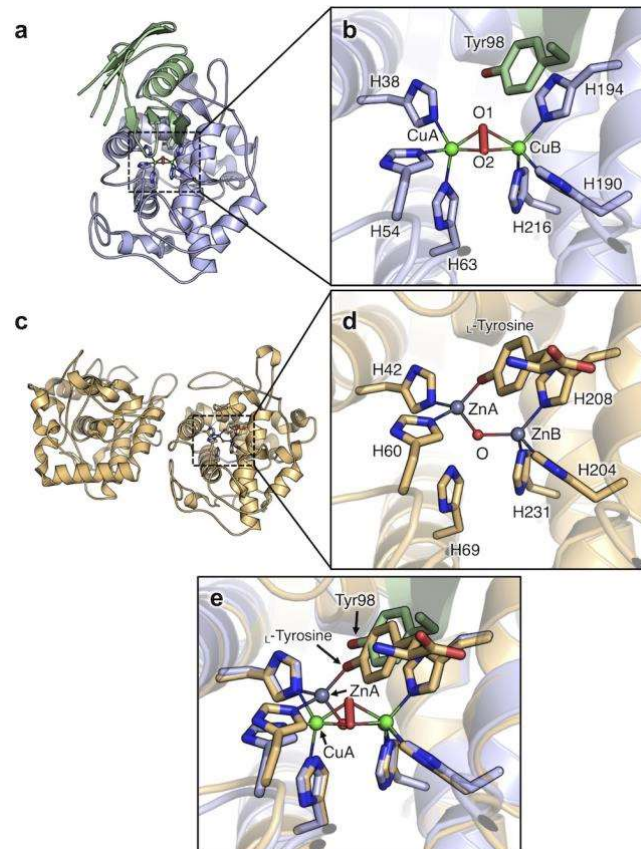
30. Emsley, P. & Cowtan, K. Coot: Model-building tools for molecular graphics. *Acta Crystallogr. Sect. D Biol. Crystallogr.* **60**, 2126–2132 (2004).
31. Thorn, A., Dittrich, B. & Sheldrick, G. M. Enhanced rigid-bond restraints. *Acta Crystallogr. Sect. A Found. Crystallogr.* **68**, 448–451 (2012).
32. Chen, V. B. *et al.* MolProbity: all-atom structure validation for macromolecular crystallography. *Acta Crystallogr. Sect. D Biol. Crystallogr.* **66**, 12–21 (2010).
33. Kabsch, W. & Sander, C. Dictionary of protein secondary structure: Pattern recognition of hydrogen-bonded and geometrical features. *Biopolymers* **22**, 2577–2637 (1983).
34. Mason, H. S. The chemistry of melanin; mechanism of the oxidation of dihydroxyphenylalanine by tyrosinase. *J. Biol. Chem.* **172**, 83–99 (1948).

Supplementary information is available for this paper at <https://doi.org/XXXXXXXXX>

Acknowledgments

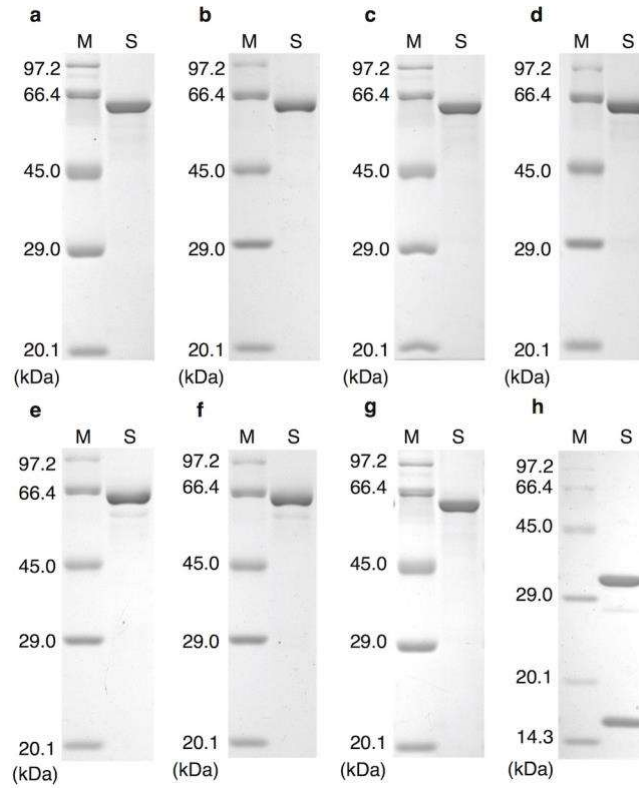
N.F. thanks JSPS, MEXT, Japan, and Kao Melanin Workshop (JSPS KAKENHI Grant Number JP15K13743 and MEXT KAKENHI Grant Number JP15H01066 and JP17H05233 in Hadean Bioscience, JP16H01025 and 18H04270 in Precisely Designed Catalysts with Customized Scaffolding). S.I. thanks JST CREST (# JPMJCR16P1). We thank Dr. E. Yamashita, Dr. A. Higashiura, and Dr. A. Nakagawa of SPring-8 BL-44XU for their support with crystallographic data collection. This work was performed in part using a synchrotron beamline BL44XU at SPring-8 under the Cooperative Research Program of Institute for Protein Research, Osaka University. Diffraction data were collected at the Osaka University beamline BL44XU at SPring-8 (Harima, Japan) under the Proposal Numbers 2014A6500, 2014B6500, 2015A6500, 2015B6500, 2016A6500, and 2016B6500.

Extended Data Figures



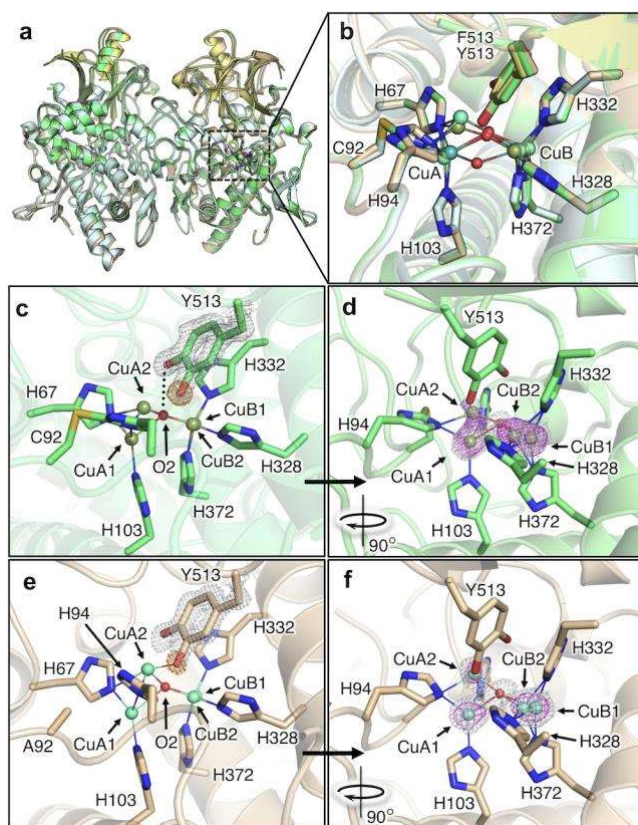
Extended Data Figure 1 | Crystal structures of the bacterial tyrosinases. **a, b,** Copper binding subunit (purple) with a caddie protein ORF378 (green) (a) and close-up of the copper centre (b) of the *Streptomyces* tyrosinase (PDB code: 1W2X). **c, d,** Dimeric structure (c) and close-up of the active site (d) of the zinc-

substituted *Bacillus* tyrosinase (PDB code: 4P6R). **e,** Superimposed active site structures of the zinc-substituted *Bacillus* tyrosinase (PDB code: 4P6R), and *Streptomyces* tyrosinase (PDB code: 1W2X). The protein main chains are displayed as ribbons, and the key amino acid residues are highlighted as sticks.



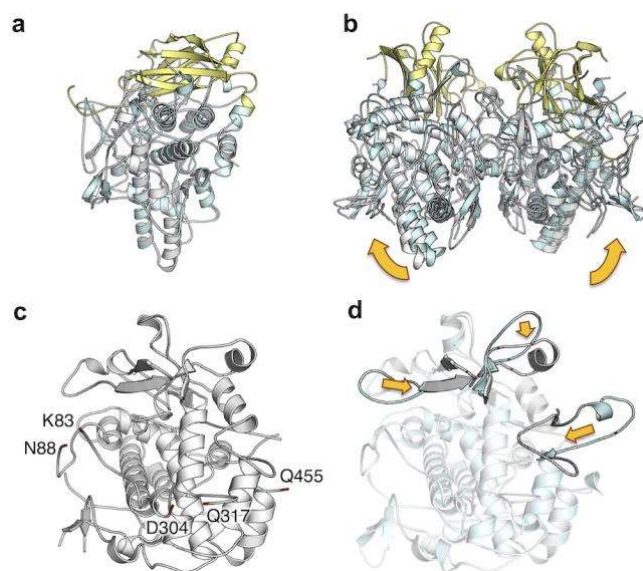
Extended Data Figure 2 | SDS-PAGE analysis of the pro-tyrosinases (12 % acrylamide) and C-terminal truncated tyrosinases (14 % acrylamide) used in this study. (a) Pro-wild type (WT); (b) Pro-F513Y; (c) Pro-C92A/F513Y; (d)

Pro-C92A (e) Pro-N333A; (f) Pro-V359A; (g) Pro-C92A/H103F; (h) Ac-C92A. M: Markers, S: Samples.



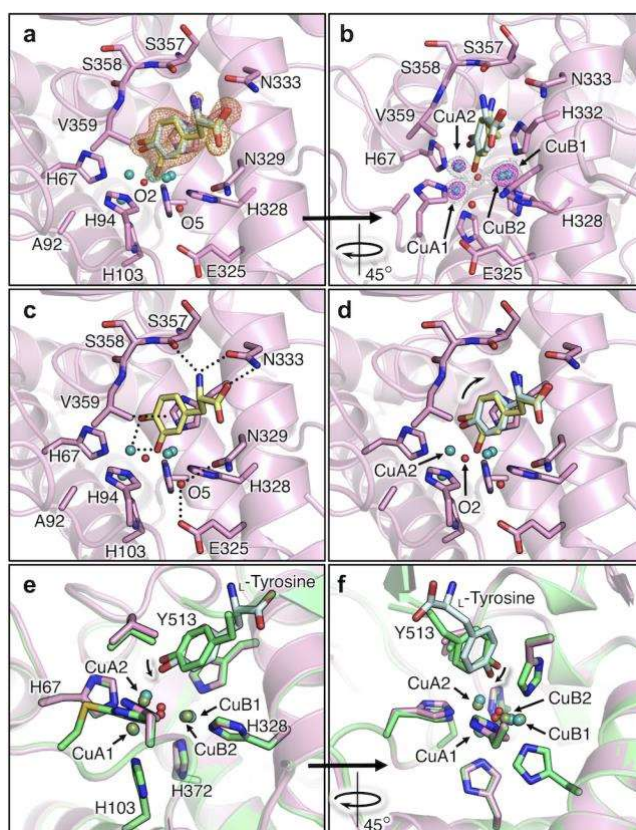
Extended Data Figure 3 | Crystal structures of the pro-forms of F513Y and C92A/F513Y mutants. **a, b,** Superimposed overall structure (**a**) and the dinuclear copper centre (**b**) of pro-F513Y (green, PDB code: 6JU4), pro-C92A/F513Y (brown, PDB code: 6JU5), and pro-wild type (blue and yellow, PDB code: 3W6W) *Aspergillus* tyrosinase. **c, d, e, f,** The copper-binding sites of

pro-F513Y (**c, d**) and pro-C92A/F513Y (**e, f**). The protein main chains are displayed as ribbons, and the key amino acid residues are highlighted as sticks. The $2Fo-Fc$, omit ($Fo-Fc$), and anomalous maps are contoured at 1.5, 3.5, and 4.5 σ and shown in gray, orange, and magenta mesh, respectively.



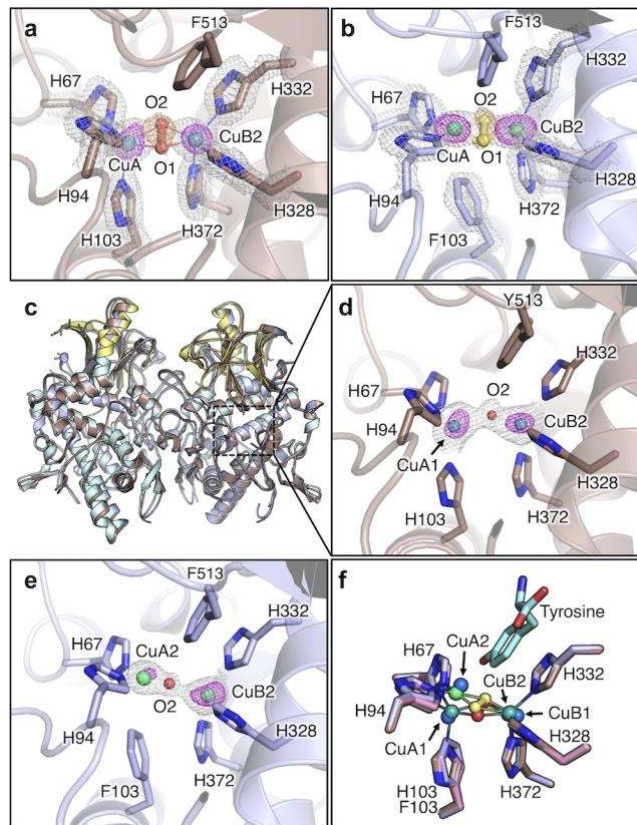
Extended Data Figure 4 | Crystal structures of the C-terminal truncated (active-form) C92A mutant. **a**, Superimposed subunit structure of pro-WT (copper-binding domain: blue, C-terminal domain: yellow) and ac-C92A (copper-depleted C-terminal truncated C92A, white). **b**, Superimposed whole-structures

of pro-WT and ac-C92A. **c**, Trypsin-cleaved site on copper-binding domain (red, Chain B). **d**, Superimposed structure of the copper-binding domains of pro-WT and ac-C92A.



Extended Data Figure 5 | Alternative crystal structures of the C-terminal truncated (active-form) C92A mutant complexed with *L*-tyrosine or *L*-DOPA. **a-d**, The structure of the substrate-binding site in ac-C92A-Cu-tyrosine (Chain A, PDB code: 6JU9). **e, f**, Superimposed structure of the substrate-binding sites of ac-C92A-Cu-tyrosine and F513Y. The protein main chains are displayed as

ribbons, and the key amino acid residues are highlighted as sticks. The *2Fo-Fc* and omit (*Fo-Fc*) maps for *L*-DOPA and *L*-Tyr, the omit map (*Fo-Fc*) for O ϵ atom of *L*-DOPA, and the anomalous map are contoured at 1.5, 4.0, 4.0, and 5.0 σ and shown in gray, orange, green, and magenta mesh, respectively.



Extended Data Figure 6 | Conventional crystal structures without consideration of radiation damage and minimum-damaged crystal structures of the pro-form of C92A and C92A/H103F mutant. a, b, The structures of the dinuclear copper centres with peroxide in the pro-C92A-Cu (Chain B, PDB code: 6JUB) (a) and pro-C92A/H103F-Cu (Chain B, PDB code: 6JUD) (b) without consideration of radiation damage. c, Superimposed overall structure of the minimum-damaged pro-C92A-Cu (PDB code: 6JUA), the minimum-damaged pro-C92A/H103F-Cu (PDB code: 6JUC), and wild type tyrosinase (PDB code: 3W6W). d, e, The structure of the dinuclear copper centres of the minimum-damaged pro-C92A-Cu (Chain A, PDB code: 6JUA)

(d), minimum-damaged pro-C92A/H103F-Cu (Chain A, PDB code: 6JUC) (e), Superimposed structure of the substrate-binding site of the minimum-damaged pro-C92A-Cu (chain B, brown), minimum-damaged pro-C92A/H103F-Cu (chain B, purple) and active-form C92A mutant [chain B of ac-C92A-cu-tyrosine (pink)]. The protein main chains are displayed as ribbons and the key amino acid residues are highlighted as sticks. The $2Fo-Fc$, omit ($Fo-Fc$), and anomalous maps are contoured at 1.8, 5.0, and 5.0 σ and shown in gray, orange, and magenta mesh, respectively.

Extended Data Tables

Extended Data Table 1 | Data Collection and Refinement Statistics.

	Pro-F513Y [6JU4]	Pro-C92A/F513Y [6JU5]	Ac-C92A [6JU6]	Ac-C92A–Tyr [6JU7]	Ac-C92A–Cu [6JU8]
Data collection					
Space group	$P2_1$	$P2_1$	$P2_12_12_1$	$P2_12_12_1$	$P2_12_12_1$
Cell dimensions					
<i>a</i> , <i>b</i> , <i>c</i> (Å)	54.22, 118.14, 79.35	54.34, 118.21, 79.36	54.28, 104.74, 154.32	54.50, 104.90, 154.74	54.15, 104.48, 154.38
α , β , γ (°)	90.00, 91.11, 90.00	90.00, 91.13, 90.00	90.00, 90.00, 90.00	90.00, 90.00, 90.00	90.00, 90.00, 90.00
Resolution (Å) [†]	50-1.35 (1.37-1.35)	50 to 1.34 (1.36-1.34)	50 to 1.50 (1.53-1.50)	50 to 1.42 (1.44-1.42)	50 to 1.27 (1.29-1.27)
No. total reflections	812649	838615	983832	1109648	1457579
No. unique reflections	217052	223775	141769	168249	230736
$R_{\text{merge}}^{\dagger}$	7.3% (67.2%)	7.6% (68.8%)	7.5% (55.4%)	8.7% (43.2%)	8.3% (51.4%)
$I / \sigma I^{\dagger}$	19.6 (2.2)	17.3 (2.1)	26.6 (3.4)	20.2 (4.5)	21.0 (3.6)
Completeness (%) [†]	99.9% (100%)	99.9% (100%)	99.6% (99.1%)	99.4% (89.6%)	99.5% (96.1%)
Redundancy [†]	3.7 (3.7)	3.8 (3.7)	7.0 (6.6)	6.6 (6.1)	6.3 (5.8)
Refinement					
Resolution (Å)	30 to 1.35	30 to 1.34	30 to 1.50	30 to 1.4	30 to 1.27
$R_{\text{work}} / R_{\text{free}}$	15.4% / 20.1%	15.7% / 20.2%	16.1% / 21.9%	15.1% / 19.4%	15.5% / 19.6%
No. atoms					
Protein	8718	8651	6978	7050	6992
Ligand/ion	0/4	0/4	4/0	30/0	4/4
Water	830	814	736	847	861
<i>B</i> -factors					
Protein	16.7	17.4	18.4	14.0	16.4
Ligand/ion	-/14.9	-/14.9	14.5/-	9.78/-	12.5/14.9
Water	26.8	27.6	28.5	25.6	27.7
R.m.s. deviations					
Bond lengths (Å)	0.0063	0.0063	0.0055	0.0064	0.0072
Bond angles (°)	1.47	1.48	1.35	1.47	1.52
	Ac-C92A–Cu–Tyr [6JU9]	Pro-C92A (oxy) [†] [6JUA]	Pro-C92A (damaged) [6JUB]	Pro-C92A/H103F (oxy) [†] [6JUC]	Pro-C92A/H103F (damaged) [6JUD]
Data collection					
Space group	$P2_1$	$P2_1$	$P2_1$	$P2_1$	$P2_1$
Cell dimensions					
<i>a</i> , <i>b</i> , <i>c</i> (Å)	54.54, 104.97, 154.88	54.72, 118.81, 79.78	53.86, 117.94, 78.32	54.12, 118.03, 79.07	54.41, 118.29, 79.55
α , β , γ (°)	90.00, 90.00, 90.00	90.00, 90.65, 90.00	90.00, 91.35, 90.00	90.00, 91.21, 90.00	90.00, 91.01, 90.00
Resolution (Å) [†]	50 to 1.42 (1.44-1.42)	50 to 1.45 (1.48-1.45)	50 to 1.54 (1.57-1.54)	50 to 1.44 (1.46-1.44)	50 to 1.56 (1.59-1.56)
No. total reflections	1147096	601044	530727	494862	541914
No. unique reflections	167605	176057	143732	179380	142070
$R_{\text{merge}}^{\dagger}$	8.7% (38.7%)	8.4% (80.4%)	8.1% (71.2%)	7.6% (74.0%)	7.8% (79.6%)
$I / \sigma I^{\dagger}$	19.2 (5.2)	12.0 (2.1)	24.3 (2.0)	13.7 (2.2)	18.7 (2.0)
Completeness (%) [†]	97.9% (96.0%)	95.1% (95.2%)	99.1% (100%)	91.4% (93.1%)	99.8% (99.4%)
Redundancy [†]	7.0 (7.0)	3.6 (3.7)	3.7 (3.8)	3.0 (3.0)	3.8 (3.8)
Refinement					
Resolution (Å)	30 to 1.42	30 to 1.45	30 to 1.54	30 to 1.44	30 to 1.56
$R_{\text{work}} / R_{\text{free}}$	15.3% / 19.6%	18.4% / 24.5%	17.4% / 23.3%	16.6% / 22.5%	16.9% / 22.8%
No. atoms					
Protein	6940	8577	8255	8534	8483
Ligand/ion	44/4	2/4	2/4	2/4	2/4
Water	743	707	486	743	692
<i>B</i> -factors					
Protein	16.2	22.3	25.0	19.9	19.3
Ligand/ion	18.8/14.5	18.6/18.9	19.6/22.1	19.2/18.2	22.6/19.7
Water	27.2	30.5	31.8	28.5	28.7
R.m.s. deviations					
Bond lengths (Å)	0.0063	0.0051	0.0048	0.0051	0.0048
Bond angles (°)	1.45	1.37	1.28	1.39	1.28

*These data were merged from 18 crystals. All other data were collected on a single crystal.

†Values in parentheses are for the highest-resolution shell.

Extended Data Table 2 | Refined occupancies and isotropic B-factors of coppers, tyrosines, and peroxides

Crystal name	Chain ID	CuA1 / CuA2 ^{††}	CuB1 / CuB2 ^{‡‡}	Tyrosine / DOPA ^{*§}	Peroxide [*]
pro-F513Y	A	59 (15.2) / 22 (21.0) [0.30]	44 (12.2) / 45 (11.8) [0.51]	23 / 77	-
	B	65 (17.1) / 17 (16.0) [0.22]	43 (13.6) / 47 (12.7) [0.52]	41 / 59	-
pro-C92A/F513Y	A	53 (15.5) / 30 (18.0) [0.36]	52 (11.7) / 42 (13.2) [0.45]	53 / 47	-
	B	52 (16.8) / 26 (17.6) [0.33]	50 (12.5) / 43 (13.5) [0.46]	42 / 58	-
ac-C92A-tyrosine [¶]	A	-	-	77 (9.1) / 0	-
	B	-	-	75 (9.6) / 0	-
ac-C92A-Cu	A	51 (14.9) / 29 (16.0) [0.36]	53 (10.9) / 40 (11.1) [0.43]	-	-
	B	59 (18.4) / 23 (19.2) [0.28]	60 (14.2) / 30 (14.4) [0.33]	-	-
ac-C92A-Cu-tyrosine [¶]	A	52 (15.9) / 37 (17.0) [0.42]	49 (11.8) / 43 (11.2) [0.47]	41 (19.9) / 46 (19.5)	-
	B	58 (16.3) / 26 (17.4) [0.31]	48 (12.7) / 42 (13.9) [0.47]	66 (18.5) / -	-
pro-C92A	A	78 (21.6)	76 (19.4)	-	-
	B	75 (17.6)	78 (16.9)	-	72 (18.6)
pro-C92A/H103F	A	51 (18.8)	83 (18.7)	-	-
	B	66 (16.1)	87 (19.1)	-	82 (19.2)

*Occupancies are given in % and B-factors are given in parentheses.

[†]CuA2-to-CuA ratios are given in brackets.

[‡]CuB2-to-CuB ratios are given in brackets.

[§]In pro-F513Y and pro-C92A/F513Y, numbers mean occupancies of Tyr513 or DOPA513.

[¶]Average B-factors are given in parentheses.

Extended Data Table 3 | Catalytic activities of tyrosinases for L-tyrosine

	His-Cys bond (Thioether)	k_{cat} (s ⁻¹)	K_m (mM)
<i>A. oryzae</i> (WT)*	Yes	82	0.090
<i>A. oryzae</i> (C92A)*	No	1.4	0.040
<i>A. oryzae</i> (N333A)*	Yes	66	1.6
<i>A. oryzae</i> (V359A)*	Yes	91	0.14
<i>A. bisporus</i> †	Yes	7.9	0.27
<i>R. solanacearum</i> ‡	No	1.4	2.1
<i>B. megaterium</i> *	No	2.5	0.075

*50 mM Potassium phosphate buffer (pH 7.0), 25 °C

†50 mM Phosphate buffer (pH 6.8), 25 °C

‡50mM Potassium phosphate (pH 7.0), 30 °C

Supplementary Information

for

Copper–oxygen dynamics in tyrosinase

Nobutaka Fujieda,^{1,2} Kyohei Umakoshi,¹ Yuta Ochi,² Yosuke Nishikawa,³ Sachiko Yanagisawa,⁴

Minoru Kubo,⁴ Genji Kurisu,³ & Shinobu Itoh¹

¹Department of Material and Life Science, Graduate School of Engineering, Osaka University, 2-1 Yamada-oka, Suita, Osaka 565-0871, Japan, ² Department of Applied Life Sciences, Graduate School of Life and Environmental Sciences, Osaka Prefecture University, 1-1 Gakuen-cho, Naka-ku, Sakai-shi, Osaka 599-8531, Japan, ³Institute for Protein Research, Osaka University, 3-2 Yamada-oka, Suita, Osaka 565-0871, Japan, ⁴Graduate School of Life Science, University of Hyogo, 3-2-1 Kouto, Kamigori-cho, Ako-gun, Hyogo 678-1297, Japan.

Supplementary Discussion

Copper plasticity in the F513Y mutants

The crystal structure of the pro-form of the F513Y mutant (pro-F513Y) was determined at a resolution of 1.35 Å with excellent statistics (Extended Data Table 1). The pro-F513Y was crystallized with one homodimer in the crystallographic asymmetric unit (space group $P2_1$). The overall structures of the pro-WT and pro-F513Y were almost identical to each other (rmsd = 0.616 Å, 1003 C α , Extended Data Fig. 3a and b). We calculated the occupancies of Tyr513 and DOPA513 and determined them to be 23 % and 77 % in chain A, and 41 % and 59 % in chain B, respectively (Extended Data Table 2). CuA1 was located at the same position of CuA in the pro-WT coordinated by the three histidines (His67, His94, and His103, Extended Data Fig. 3c). In stark contrast, newly emerging CuA2 was 1.80 Å and 1.83 Å (Supplementary Table 3) away from CuA1 in chain A and B, respectively, and it was coordinated by Tyr513 or oxidized Try513, DOPA513 as well as two histidines (His67 and His94). In this case, His103 is detached from the copper ion (Extended Data Fig. 3c). Occupancies by CuA1 and CuA2 were determined to be 59 % and 22 % in chain A, and 65 % and 17 % in chain B, respectively (Extended Data Table 2). Surprisingly, elongated anomalous peaks due to copper ion (CuB1 and CuB2) were also observed at the CuB site (His328, His332, and His372, Extended Data Fig. 3d). CuB2 sat at the same position of CuB in the pro-WT supported by the three histidines (His328, His332, and His372, Extended Data Fig. 3d). On the other hand, CuB1 was 1.03 Å and 0.97 Å away from CuB2 in chain A and B, respectively, shifting toward the N ϵ atoms of His328 and His332. Occupancies by CuB1 and CuB2 were determined to be 47 % and 45 % in chain A, and 47 % and 43 % in chain B, respectively (Extended Data Table 2). Whereas the distance between CuA1 and CuB1 is 4.43 Å, the distance between CuA2 and CuB2 is 3.20 Å in chain A (4.43 Å and 3.24 Å in chain B, respectively). Between the coppers, one water molecule (O2) is hydrogen-bonded to the oxygen atom of Tyr513 and is present at a closer position to CuB2 than that of the pro-WT (1.73 Å, Supplementary Table 3).

His-Cys cross-linkage

In the *Aspergillus* tyrosinase, Cys92 is covalently bound to His94, one of the CuA-ligands, forming a His-Cys cross-link^{1,2} as in the *Agaricus bisporus* tyrosinase³. The cross-linkage may contribute to the catalytic activity based on the results of our previous enzymatic assay¹, but many tyrosinases from *Bacillus megaterium*⁴, *R. solanacearum*⁵, and *Streptomyces castaneoglobisporus*⁶ do not have this cross-link. Thus, it appears somewhat redundant for the catalytic activity (Extended Data Table 3). Eventually, the C92A mutant exhibits lower activity toward L-tyrosine than WT, but it still keeps comparable phenolase activity,

in comparison with those of other tyrosinases with⁷ or without^{8,9} the His-Cys cross-link reported previously under comparable conditions (Extended Data Table 3).

Copper plasticity in the C92A/F513Y mutants

The Cys92Ala/Phe513Tyr mutant (C92A/F513Y without the His-Cys cross-link) showed the same phenomena as pro-F513Y. The crystal structure of pro-C92A/F513Y was determined at a resolution of 1.34 Å with excellent statistics (Extended Data Table 1). Pro-C92A/F513Y was crystallized with one homodimer in the crystallographic asymmetric unit (space group $P2_1$). Overall structures of pro-C92A/F513Y were almost identical with those of pro-WT (rmsd = 0.614 Å, 995 C α) and pro-F513Y (rmsd = 0.092 Å, 1008 C α) (Extended Data Fig. 3a, b). The additional electron density was observed at the ortho-position of the phenol ring of Tyr513 (Extended Data Fig. 3e). We calculated the occupancies of Tyr513 and DOPA513 and determined them to be 53 % and 47% in chain A, and 42 % and 58% in chain B, respectively (Extended Data Table 2). Furthermore, two distinct electron densities corresponding to the copper ions (CuA1 and CuA2) were observed as well (Extended Data Fig. 3e, f). The elongated anomalous peaks deriving from the copper ions (CuB1 and CuB2) were also observed at the CuB site (His328, His332, and His372; Extended Data Fig. 3f). The location of the aromatic rings of Tyr513 and DOPA513 in both pro-F513Y and pro-C92A/F513Y coincided exactly with that of Phe513 in pro-WT in the superimposed structure, suggesting that rotation and transition of DOPA513 were not induced by the hydroxylation of Tyr513 (Extended Data Fig. 3b). This situation is completely different from the case of the bound substrate (see below, the section “Hydroxylation of bound L-tyrosine”).

The overall structure of active-form of the C92A mutant

To obtain the active-form of the C92A mutant (ac-C92A), the pro-C92A (copper-depleted form) was treated with trypsin. Then, the resultant solution was subjected to anion exchange chromatography to remove the digested small peptides. The protein exhibited two bands on SDS-PAGE as previously reported (Extended Data Fig. 2h)¹⁰. Based on the results of previous studies¹⁰, the two major bands (38 kDa and 18 kDa) were assigned to the fragments of the copper-binding domain Gly(-4)–Lys312 and Asn313–Lys457, respectively. Although the previous activation procedure still resulted in the slightly auto-oxidation of the C92A mutant, the elongated trypsin treatment at low temperature and subsequently single step purification allowed us to obtain the high-quality ac-tyrosinase crystals (see Methods). Finally, we succeeded to crystallize ac-C92A without any tyrosinase inhibitor. In the asymmetric unit (space group $P2_12_12_1$), the two monomers, which are indeed separated into two polypeptides as described in the former paragraph, were associated in a pseudo-homodimeric structure related by a 2-fold symmetry and interacted with each other in a back-to-back fashion, displaying an ellipsoid shape with the dimensions of

85 Å × 55 Å × 45 Å (Fig. 2a and Extended Data Fig. 4). The monomer is composed of 461 amino acid residues, most of which were well defined in the model (Supplementary Table 1), and almost no structural change was observed in the core structure (four-helix bundle) in comparison with the copper-binding domain of pro-WT (rmsd = 0.233, 324 C_α, Chain A in pro-WT vs. Chain B in ac-C92A; Extended Data Fig. 4a). The electron density corresponding to the C-terminal domain was not observed, indicative of its complete removal by purification after trypsin treatment. The pseudo-dimeric structure of ac-C92A was slightly deviated from that of the copper-binding domain of pro-WT (rmsd = 1.961, 759 C_α), where each monomer rotated by 5° to fill the space that had been occupied by the C-terminal domain in the pro-WT (Extended Data Fig. 4b). In support of this notion, the interaction area became smaller than that of pro-WT (from 2.0 × 10³ Å² to 1.4 × 10³ Å²), and a nitrate ion was observed in the interaction area. The cleaved site on the copper-binding domain (Lys312–Asn313) were disordered in ac-C92A same as in pro-WT, indicating that these regions do not contribute to the folding of the core structures (Extended Data Fig. 4c, red residues). Meanwhile, the conformations of the three loops changed to fill the space that would be occupied by the C-terminal domain in the pro-WT (Ala210–Pro226, Asn262–Leu279, and Gly336–Gly352; Extended Data Fig. 4d). The crystal structures of the binary complex (ac-C92A–tyrosine and ac-C92A–Cu) and ternary complex (ac-C92A–Cu–tyrosine) were obtained by soaking the ac-C92A crystals with L-tyrosine and/or copper sulphate. Naturally, these four crystals have one homodimer in the crystallographic asymmetric unit (space group *P*2₁2₁2₁), and the overall structures of ac-C92A–tyrosine, ac-C92A–Cu, and ac-C92A–Cu–tyrosine were almost the same as that of ac-C92A (rmsd = 0.083 Å (751 C_α), 0.061 Å (748 C_α), and 0.086 Å (750 C_α), respectively, Fig. 2a).

Hydroxylation of the bound L-tyrosine

The electron density resulting from the O ϵ of L-DOPA was seen only in the chain A of ac-C92A–Cu–tyrosine, but not in the chain B. The binding mode of L-DOPA in the chain A was almost identical with that of L-tyrosine, except that the catechol moiety coordinated to CuA2 in the bidentate fashion (2.36 and 2.13 Å, CuA2–O ζ and CuA2–O ϵ , respectively, Extended Data Fig. 5a-5d), and thus the catechol moiety was rotated by > 10° (Extended Data Fig. 5d).

Crystal structures of the dioxygen-bound form

We crystallized copper-depleted pro-C92A and copper-depleted pro-C92A/H103F followed by soaking in the cryoprotectant solution containing CuSO₄ to obtain the structures of the oxy-forms of both mutants [pro-C92A-copper-dioxygen (pro-C92A–Cu) and pro-C92A/H103F-copper-dioxygen (pro-C92A/H103F–Cu) ternary complexes], and resolved their structures at resolutions of 1.54 Å and 1.56 Å, respectively, with excellent statistics (Extended Data Table 1 and Supplementary Table 2). However, the

pro-C92A–Cu structure did not have a clear electron density corresponding to the peroxide species in the metal centre (Extended Data Fig. 6a) and retained ambiguous electron density between CuA and CuB. In support of these results, the O–O bond length of the peroxide refined without any geometrical restraint was 1.61 Å, which is somewhat longer than that of peroxide as previously reported (1.41–1.48 Å)¹¹. Similarly, such elongation of the O–O bond length was observed (1.63 Å) in the case of pro-C92A/H103F–Cu (Extended Data Fig. 6b). These results indicated that the excess exposure of the crystals to strong X-ray beams induced photo-reduction of a peroxide species.

To reduce the X-ray damage of the crystals, the diffraction data were collected and merged by using multiple crystals. As the number of the crystals increased, the electron density between the two copper ions clearly appeared. Finally, the low X-ray-dosed crystal structures of pro-C92A–Cu and pro-C92A/H103F–Cu determined by using 18 crystals were obtained at the resolutions of 1.45 Å and 1.44 Å, respectively (Fig. 3c and d, and Extended Data Fig. 6c–6e). The whole structures of pro-C92A–Cu and pro-C92A/H103F–Cu were almost the same as that of pro-WT [rmsd = 0.612, 989 C_α (pro-C92A–Cu vs. pro-WT) and 0.619, 1010 C_α (pro-C92A/H103F–Cu vs. pro-WT), 0.277, 1037 C_α (pro-C92A–Cu vs. pro-C92A/H103F–Cu), respectively] (Extended Data Fig. 6c). Eventually, the electron density between the copper ions resulting from the peroxide bridge was observed only in the chain B, and the copper centre in the chain A had one oxygen atom presumably deriving from a water molecule, indicating that the crystal packing slightly changed each conformation to assume different states.

The coordination geometry of the Cu₂O₂ core

In the chain B of pro-C92A–Cu crystal, both copper sites adopted distorted square pyramidal geometry with the geometry index τ_5 values (CuA: $\tau_5 = 0.29$, CuB: $\tau_5 = 0.057$), where His103 and His372 were situated in axial positions. The Cu₂O₂ core exhibited a symmetrical diamond structure, similar to those of the previously reported (μ - η^2 : η^2 -peroxido)dicopper(II) species in the model compounds.¹¹ On the other hand, the Cu₂O₂ core of pro-C92A/H103F–Cu showed clearly asymmetric (μ - η^2 : η^2 -peroxido)dicopper(II) structure, reflecting the difference of the ligands of each copper. CuA had a square planar geometry ($\tau_4 = 0.23$) composed of two histidines and peroxide ion ligands, and CuB had nearly square pyramidal geometry ($\tau_5 = 0.12$) as in the case of pro-C92A–Cu.

So far, crystal structures of the oxy-form in tyrosinases have been refined with the strong geometrical constraints for the peroxide ion so that the O–O bond length was forced to be approximately 1.47 Å according to that of the peroxide ion and model compounds¹¹. Therefore, the reported oxy-form structures of the *Streptomyces* tyrosinase (PDB code: 1WX2, 1.80 Å resolution, Extended Data Fig. 1b)⁶ showed the O–O bond length of 1.48 Å, which is around the reported value of 1.47 Å. On the other hand, the crystal structure of the arthropod tyrosinase (PDB code: 3WKY, 1.80 Å resolution) contains a Cu₂O₂ core

bearing O–O bond at 1.66 Å because of no restraints on the O–O bond, suggesting that photo-reduction reaction took place due to the high X-ray irradiation. Our results from the oxy-form crystals (pro-C92A–Cu and pro-C92A/H103F–Cu) are the first examples of (μ - η^2 : η^2 -peroxido)dicopper(II) structure in proteins at a higher resolution than 1.5 Å calculated with no geometrical restraints to the Cu₂O₂ core including the O–O bond restraint, and these results will provide us profound insights about the properties of reactive copper-oxygen species as well as the mechanisms of non-haem dinuclear metalloenzymes.

1. Fujieda, N. *et al.* Post-translational His-Cys cross-linkage formation in tyrosinase induced by copper(II)-peroxo species. *J. Am. Chem. Soc.* **133**, 1180–1183 (2011).
2. Fujieda, N. *et al.* Crystal structures of copper-depleted and copper-bound fungal pro-tyrosinase: insights into endogenous cysteine-dependent copper incorporation. *J. Biol. Chem.* **288**, 22128–40 (2013).
3. Ismaya, W. T. *et al.* Crystal structure of *Agaricus bisporus* mushroom tyrosinase: Identity of the tetramer subunits and interaction with tropolone. *Biochemistry* **50**, 5477–86 (2011).
4. Sendovski, M., Kanteev, M., Ben-Yosef, V. S., Adir, N. & Fishman, A. First structures of an active bacterial tyrosinase reveal copper plasticity. *J. Mol. Biol.* **405**, 227–37 (2011).
5. Hernández-Romero, D., Sanchez-Amat, A. & Solano, F. A tyrosinase with an abnormally high tyrosine hydroxylase/dopa oxidase ratio: Role of the seventh histidine and accessibility to the active site. *FEBS J.* **273**, 257–270 (2006).
6. Matoba, Y., Kumagai, T., Yamamoto, A., Yoshitsu, H. & Sugiyama, M. Crystallographic evidence that the dinuclear copper center of tyrosinase is flexible during catalysis. *J. Biol. Chem.* **281**, 8981–90 (2006).
7. Espín, J. C., García-Ruiz, P. A., Tudela, J. & García-Cánovas, F. Study of stereospecificity in mushroom tyrosinase. *Biochem. J.* **331** (Pt 2, 547–51 (1998).
8. Molloy, S. *et al.* Engineering of a bacterial tyrosinase for improved catalytic efficiency towards D-tyrosine using random and site directed mutagenesis approaches. *Biotechnol. Bioeng.* **110**, 1849–57 (2013).
9. Shuster, V. & Fishman, A. Isolation, cloning and characterization of a tyrosinase with improved activity in organic solvents from *Bacillus megaterium*. *J. Mol. Microbiol. Biotechnol.* **17**, 188–200 (2009).
10. Fujieda, N. *et al.* Multifunctions of *MelB*, a fungal tyrosinase from *Aspergillus oryzae*.

Chembiochem **13**, 193–201 (2012).

11. Mirica, L. M., Ottenwaelder, X. & Stack, T. D. P. Structure and spectroscopy of copper-dioxygen complexes. *Chem. Rev.* **104**, 1013–45 (2004).

Supplementary Tables

Supplementary Table 1 | Oligonucleotides used for site-directed mutagenesis of tyrosinase

No.	Sequence (5'-3')	Length	Use
1	AGCGGCAGCCTTGAGGACAGTAACTG	26	Forward primer for F513Y
2	<u>ATAG</u> TTGAAGACACTGCCACAAAATTCTG	30	Reverse primer for F513Y
3	<u>GCA</u> TGGGTGGGAGGATTCATGTTTCAGC	27	Forward primer for N333A
4	ATGGACGTTGTTGTGAATAGCTTCTAAGTTC	31	Reverse primer for N333A
5	CCAGTGGCCGCGTATGATCCGATTTTC	27	Forward primer for V359A
6	<u>TGC</u> ACTGCTCATATGGCCAGCACCCCAG	28	Reverse primer for V359A
7	<u>TTTC</u> GGGTGTATGTGACCTTGACG	25	Forward primer for H103F
8	CCATGTCGGAAAGGTGTAATTG	22	Reverse primer for H103F

*The mutagenic nucleotides are underlined.

Supplementary Table 2 | Missing residues and atoms

Pro-F513Y (PDB code: 6JU4)

Missing residues

Chain A: Gly(-3)–Gly0, Gly80–Pro88, His154–Gly161, Ser213–Phe223, Lys305–Gln316, Arg455–Glu465, Ser516–Cys525, Glu584–Asp597

Chain B: Ser31–Asn35, His154–Gly161, Gln214–Trp221, Asp304–Gln316, Gly515–Gly532, Ala590–Asp597

Missing atoms

Chain A: Lys13 (C δ , C ϵ , N ζ), Ser34 (O γ), Lys123 (C γ , C δ , C ϵ , N ζ), Gln128 (C γ , C δ , O ϵ 1, N ϵ 2), Arg153 (C γ , C δ , N ϵ , C ζ , N η 1, N η 2), Lys176 (C γ , C δ , C ϵ , N ζ), Gln182 (C γ , C δ , O ϵ 1, N ϵ 2), Pro183 (C β , C γ , C δ), Lys185 (C γ , C δ , C ϵ , N ζ), Leu187 (C γ , C δ 1, C δ 2), Glu206 (C γ , C δ , O ϵ 1, O ϵ 2), Arg207 (C γ , C δ , N ϵ , C ζ , N η 1, N η 2), Asp224 (C γ , O δ 1, O δ 2), Lys229 (C γ , C δ , C ϵ , N ζ), Asp271 (C γ , O δ 1, O δ 2), Lys319 (C γ , C δ , C ϵ , N ζ), Asp394 (C γ , O δ 1, O δ 2), Lys397 (C γ , C δ , C ϵ , N ζ), Glu412 (C γ , C δ , O ϵ 1, O ϵ 2), Lys413 (C γ , C δ , C ϵ , N ζ), Arg415 (C γ , C δ , N ϵ , C ζ , N η 1, N η 2), Lys416 (C γ , C δ , C ϵ , N ζ), Asp440 (C γ , O δ 1, O δ 2), Arg443 (C γ , C δ , N ϵ , C ζ , N η 1, N η 2), Arg445 (C γ , C δ , N ϵ , C ζ , N η 1, N η 2), Glu447 (C γ , C δ , O ϵ 1, O ϵ 2), Ser449 (O γ), Gln454 (C γ , C δ , O ϵ 1, N ϵ 2), Glu466 (C γ , C δ , O ϵ 1, O ϵ 2), Lys496 (C δ , C ϵ , N ζ), Gln527 (C γ , C δ , O ϵ 1, N ϵ 2), Glu531 (C δ , O ϵ 1, O ϵ 2), Arg542 (C ζ , N η 1, N η 2), Lys550 (C δ , C ϵ , N ζ), Lys553 (C δ , C ϵ , N ζ), Arg560 (C γ , C δ , N ϵ , C ζ , N η 1, N η 2), Asp598 (C β , C γ , O δ 1, O δ 2), Arg600 (C γ , C δ , N ϵ , C ζ , N η 1, N η 2), Arg601 (N ϵ , C ζ , N η 1, N η 2), Lys606 (C γ , C δ , C ϵ , N ζ), Glu609 (C γ , C δ , O ϵ 1, O ϵ 2), Arg615 (C γ , C δ , N ϵ , C ζ , N η 1, N η 2)

Chain B: Ser1 (O γ), Lys10 (C γ , C δ , C ϵ , N ζ), Lys13 (C γ , C δ , C ϵ , N ζ), Glu28 (C γ , C δ , O ϵ 1, O ϵ 2), Lys82 (C β , C γ , C δ , C ϵ , N ζ), Asp83 (C β , C γ , O δ 1, O δ 2), Ser84 (O γ), Lys85 (C β , C γ , C δ , C ϵ , N ζ), Asn87 (C γ , O δ 1, N δ 2), Lys123 (C ϵ , N ζ), Gln128 (C γ , C δ , O ϵ 1, N ϵ 2), Lys139 (N ζ), Arg153 (C γ , C δ , N ϵ , C ζ , N η 1, N η 2), Asp162 (C γ , O δ 1, O δ 2), Gln182 (C γ , C δ , O ϵ 1, N ϵ 2), Lys185 (C γ , C δ , C ϵ , N ζ), Glu206 (C γ , C δ , O ϵ 1, O ϵ 2), Arg207 (C δ , N ϵ , C ζ , N η 1, N η 2), Thr212 (O γ 1, O γ 2), Ser222 (C β , O γ), Asp303 (C γ , O δ 1, O δ 2), Pro318 (C γ , C δ), Lys319 (C γ , C δ , C ϵ , N ζ), Arg345 (N ϵ , C ζ , N η 1, N η 2), Lys395 (C γ , C δ , C ϵ , N ζ), Lys397 (C γ , C δ , C ϵ , N ζ), Glu412 (C γ , C δ , O ϵ 1, O ϵ 2), Lys413 (C γ , C δ , C ϵ , N ζ), Arg415 (C γ , C δ , N ϵ , C ζ , N η 1, N η 2), Lys416 (C γ , C δ , C ϵ , N ζ), Asp440 (C γ , O δ 1, O δ 2), Arg443 (C γ , C δ , N ϵ , C ζ , N η 1, N η 2), Lys446 (C γ , C δ , C ϵ , N ζ), Glu447 (C γ , C δ , O ϵ 1, O ϵ 2), Lys461 (C γ , C δ , C ϵ , N ζ), Glu465 (C γ , C δ , O ϵ 1, O ϵ 2), Arg476 (N ϵ , C ζ , N η 1, N η 2), Tyr477 (C γ , C δ 1, C δ 2, C ϵ 1, C ϵ 2, C ζ , O η), Lys482 (C γ , C δ , C ϵ , N ζ), Lys553 (C γ , C δ , C ϵ , N ζ), Glu555 (C γ , C δ , O ϵ 1, O ϵ 2), Glu584 (C γ , C δ , O ϵ 1, O ϵ 2), Arg600 (C γ , C δ , N ϵ , C ζ , N η 1, N η 2), Lys606 (C γ , C δ , C ϵ , N ζ), Glu609 (C δ , O ϵ 1, O ϵ 2)

Pro-C92A/F513Y (PDB code: 6JU5)

Missing residues

Chain A: Gly(-3)–Gly0, Gly80–Pro88, His154–Gly161, Ser213–Trp221, Lys305–Gln316, Gln454–Glu465, Ser516–Cys525, Glu584–Asp597

Chain B: Ser31–Asn35, Gly80–Gly86, His154–Gly161, Ser213–Trp221, Asp304–Gln316, Gly515–Gly532, Pro591–Ser596

Missing atoms

Chain A: Ser1 (O γ), Lys13 (C δ , C ϵ , N ζ), Ser34 (O γ), Thr89 (O γ 1, O γ 2), Gln128 (C γ , C δ , O ϵ 1, N ϵ 2), Arg153 (C γ , C δ , N ϵ , C ζ , N η 1, N η 2), Asp162 (C γ , O δ 1, O δ 2), Lys176 (C γ , C δ , C ϵ , N ζ), Gln182 (C γ , C δ , O ϵ 1, N ϵ 2), Pro183 (C γ , C δ), Lys185 (C γ , C δ , C ϵ , N ζ), Leu187 (C γ , C δ 1, C δ 2), Glu206 (C γ , C δ , O ϵ 1, O ϵ 2), Arg207 (C γ , C δ , N ϵ , C ζ , N η 1, N η 2), Thr212 (O γ 1, O γ 2), Ser222 (O γ), Asp224 (C γ , O δ 1, O δ 2), Lys229 (C δ , C ϵ , N ζ), Asp271 (C γ , O δ 1, O δ 2), Asp274 (C γ , O δ 1, O δ 2), Asp303 (C γ , O δ 1, O δ 2), Asp304 (C γ , O δ 1, O δ 2), Ala317 (C β), Pro318 (C β , C γ , C δ), Lys319 (C γ , C δ , C ϵ , N ζ), Arg345 (C γ , C δ , N ϵ , C ζ , N η 1, N η 2), Asp347 (C γ , O δ 1, O δ 2), Asp394 (C γ , O δ 1, O δ 2), Lys397 (C γ , C δ , C ϵ , N ζ), Glu412 (C δ , O ϵ 1, O ϵ 2), Lys413 (C γ , C δ , C ϵ , N ζ), Arg415 (C γ , C δ , N ϵ , C ζ , N η 1, N η 2), Lys416 (C γ , C δ , C ϵ , N ζ), Arg443 (C γ , C δ , N ϵ , C ζ , N η 1, N η 2), Arg445 (C γ , C δ , N ϵ , C ζ , N η 1, N η 2), Lys446 (C γ , C δ , C ϵ , N ζ), Glu447 (C γ , C δ , O ϵ 1, O ϵ 2), Glu466 (C γ , C δ , O ϵ 1, O ϵ 2), Lys482 (C δ , C ϵ , N ζ), Gln527 (C γ , C δ , O ϵ 1, N ϵ 2), Glu531 (C γ , C δ , O ϵ 1, O ϵ 2), Arg542 (N ϵ , C ζ , N η 1, N η 2), Lys553 (C δ , C ϵ , N ζ), Arg560 (N ϵ , C ζ , N η 1, N η 2), Glu573 (C γ , C δ , O ϵ 1, O ϵ 2), Lys575 (C δ , C ϵ , N ζ), Glu577 (C γ , C δ , O ϵ 1, O ϵ 2), Asp598 (C β , C γ , O δ 1, O δ 2), Arg600 (C γ , C δ , N ϵ , C ζ , N η 1, N η 2), Arg601 (C δ , N ϵ , C ζ , N η 1, N η 2), Lys606 (C γ , C δ , C ϵ , N ζ), Asp612 (C γ , O δ 1, O δ 2), Arg615 (C γ , C δ , N ϵ , C ζ , N η 1, N η 2)

Chain B: Ser1 (O γ), Lys10 (C δ , C ϵ , N ζ), Lys13 (C γ , C δ , C ϵ , N ζ), Glu28 (C γ , C δ , O ϵ 1, O ϵ 2), Asn87 (C β , C γ , O δ 1, N δ 2), Pro88 (C γ , C δ), Gln128 (C γ , C δ , O ϵ 1, N ϵ 2), Arg153 (C γ , C δ , N ϵ , C ζ , N η 1, N η 2), Asp162 (C γ , O δ 1, O δ 2), Lys176 (C δ , C ϵ , N ζ), Gln182 (C δ , O ϵ 1, N ϵ 2), Lys185 (C γ , C δ , C ϵ , N ζ), Glu206 (C γ , C δ , O ϵ 1, O ϵ 2), Arg207 (C δ , N ϵ , C ζ , N η 1, N η 2), Phe223 (C γ , C δ 1, C δ 2, C ϵ 1, C ϵ 2, C ζ), Asn241 (C γ , O δ 1, N δ 2), Asp303 (C γ , O δ 1, O δ 2), Pro318 (C γ , C δ), Lys319 (C γ , C δ , C ϵ , N ζ), Arg345 (C γ , N ϵ , C ζ , N η 1, N η 2), Asp347 (C γ , O δ 1, O δ 2), Lys395 (C γ , C δ , C ϵ , N ζ), Lys397 (C γ , C δ , C ϵ , N ζ), Glu412 (C γ , C δ , O ϵ 1, O ϵ 2), Lys413 (C γ , C δ , C ϵ , N ζ), Arg415 (C γ , C δ , N ϵ , C ζ , N η 1, N η 2), Lys416 (C γ , C δ , C ϵ , N ζ), Asp440 (C γ , O δ 1, O δ 2), Arg443 (C γ , C δ , N ϵ , C ζ , N η 1, N η 2), Lys446 (C γ , C δ , C ϵ , N ζ), Glu447 (C γ , C δ , O ϵ 1, O ϵ 2), Lys461 (C γ , C δ , C ϵ , N ζ), Glu465 (C γ , C δ , O ϵ 1, O ϵ 2), Glu466 (C γ , C δ , O ϵ 1, O ϵ 2), Arg476 (N ϵ , C ζ , N η 1, N η 2), Tyr477 (C γ , C δ 1, C δ 2, C ϵ 1, C ϵ 2, C ζ , O η), Lys482 (C γ , C δ , C ϵ , N ζ), Ser514 (O γ), Glu555 (C γ , C δ , O ϵ 1, O ϵ 2), Lys582 (C ϵ , N ζ), Glu584 (C γ , C δ , O ϵ 1, O ϵ 2), Ala590 (C β), Asp597 (C γ , O δ 1, O δ 2), Arg600 (C γ , C δ , N ϵ , C ζ , N η 1, N η 2), Lys606 (C γ , C δ , C ϵ , N ζ), Asp612 (C γ , O δ 1, O δ 2)

Ac-C92A (PDB code: 6JU6)

Missing residues

Chain A: Gly(-3)–Gly0, His156–Gln160, Thr309–Lys319, Gln454–Lys457

Chain B: Gly(-3)–Gly(-1), Asp83–Gly86, His156–Gly161, Asp304–Glu315, Glu412–Arg415, Arg455–Lys457

Missing atoms

Chain A: Ser1 (O γ), Lys10 (C δ , C ϵ , N ζ), Lys13 (C γ , C δ , C ϵ , N ζ), Ser31 (O γ), Ala32(C β), Ser34 (O γ), Gln81 (C γ , C δ , O ϵ 1, N ϵ 2), Lys82 (C δ , C ϵ , N ζ), Lys123 (C γ , C δ , C ϵ , N ζ), Lys176 (C γ , C δ , C ϵ , N ζ), Lys185 (C γ , C δ , C ϵ , N ζ), Arg207 (C γ , C δ , N ϵ , C ζ , N η 1, N η 2), Asp274 (C γ , O δ 1, O δ 2), Asp303 (C γ , O δ 1, O δ 2), Lys305 (C γ , C δ , C ϵ , N ζ), Lys306 (C γ , C δ , C ϵ , N ζ), Glu308 (C β , C γ , C δ , O ϵ 1, O ϵ 2), Arg345 (C γ , C δ , N ϵ , C ζ , N η 1, N η 2), Glu412 (C γ , C δ , O ϵ 1, O ϵ 2), Lys413 (C β , C γ , C δ , C ϵ , N ζ)

Chain B: Ser1 (C β , O γ), Lys82 (C γ , C δ , C ϵ , N ζ), Asn87 (C γ , O δ 1, N δ 2), Arg153 (C γ , C δ , N ϵ , C ζ , N η 1, N η 2), Lys185 (C β , C γ , C δ , C ϵ , N ζ), Leu187(C γ , C δ 1, C δ 2), Gln199 (C γ , C δ , O ϵ 1, N ϵ 2), Arg207 (C γ , C δ , N ϵ , C ζ , N η 1, N η 2), Trp221 (C γ , C δ 1, C δ 2, N ϵ 1, C ϵ 2, C ϵ 3, C ζ 2, C ζ 3, C η 2), Asp271 (C γ , O δ 1, O δ 2), Arg301 (N ϵ , C ζ , N η 1, N η 2), Gln316 (C γ , C δ , O ϵ 1, N ϵ 2), Arg345 (C γ , C δ , N ϵ , C ζ , N η 1, N η 2), Asn392 (C γ , O δ 1, N δ 2), Lys397 (C γ , C δ , C ϵ , N ζ), Phe410 (C γ , C δ 1, C δ 2, C ϵ 1, C ϵ 2, C ζ), Lys416 (C β , C γ , C δ , C ϵ , N ζ), Ser442 (O γ), Gln454 (C β , C γ , C δ , O ϵ 1, N ϵ 2)

Ac-C92A-tyrosine (PDB code: 6JU7)

Missing residues

Chain A: Gly(-3)-Gly0, His156-Asn158, Lys306-Pro318, Gln454-Lys457

Chain B: Gly(-3)-Gly(-1), Thr159-Gly161, Asp304-Glu315, Glu412-Lys413, Arg455-Lys457

Missing atoms

Chain A: Lys13 (C γ , C δ , C ϵ , N ζ), Gln81 (C γ , C δ , O ϵ 1, N ϵ 2), Lys82 (C γ , C δ , C ϵ , N ζ), Gln128 (C γ , C δ , O ϵ 1, N ϵ 2), Thr159 (O γ 1, O γ 2), Gln160 (C β , C γ , C δ , O ϵ 1, N ϵ 2), Lys176 (C γ , C δ , C ϵ , N ζ), Pro183 (C γ , C δ), Lys185 (C γ , C δ , C ϵ , N ζ), Arg207 (C γ , C δ , N ϵ , C ζ , N η 1, N η 2), His219 (C γ , N δ 1, C δ 2, C ϵ 1, N ϵ 2), Asp271 (C γ , O δ 1, O δ 2), Asp274 (C γ , O δ 1, O δ 2), Lys305 (C γ , C δ , C ϵ , N ζ), Arg345 (C γ , C δ , N ϵ , C ζ , N η 1, N η 2), Glu412 (C γ , C δ , O ϵ 1, O ϵ 2), Lys413 (C β , C γ , C δ , C ϵ , N ζ), Thr414 (O γ 1, O γ 2), Arg415 (C γ , C δ , N ϵ , C ζ , N η 1, N η 2)

Chain B: Lys10 (C γ , C δ , C ϵ , N ζ), Lys82 (C γ , C δ , C ϵ , N ζ), Asp83 (C γ , O δ 1, O δ 2), Ser84 (C β , O γ), Lys82 (C β , C γ , C δ , C ϵ , N ζ), Arg153 (C γ , C δ , N ϵ , C ζ , N η 1, N η 2), His154 (C γ , N δ 1, C δ 2, C ϵ 1, N ϵ 2), Leu187 (C γ , C δ 1, C δ 2), Arg207 (C γ , C δ , N ϵ , C ζ , N η 1, N η 2), Asp271 (C γ , O δ 1, O δ 2), Arg301 (N ϵ , C ζ , N η 1, N η 2), Gln316 (C β , C γ , C δ , O ϵ 1, N ϵ 2), Thr414 (O γ 1, O γ 2), Arg415 (C γ , C δ , N ϵ , C ζ , N η 1, N η 2), Lys416 (C γ , C δ , C ϵ , N ζ), Ser442 (O γ), Arg445 (C δ , N ϵ , C ζ , N η 1, N η 2), Gln454 (C γ , C δ , O ϵ 1, N ϵ 2)

Ac-C92A–Cu (PDB code: 6JU8)

Missing residues

Chain A, Gly(-3)–Gly0, His156-Gln160, Glu308-Pro318, Gln454-Lys457

Chain B, Gly(-3)–Pro(-2), Lys82-Lys85, His156-Gly161, Asp304-Gln316, Arg455-Lys457

Missing atoms

Chain A: Ser1 (O γ), Lys10 (C γ , C δ , C ϵ , N ζ), Pro12 (C γ , C δ), Lys13 (C γ , C δ , C ϵ , N ζ), Gln81 (C γ , C δ , O ϵ 1, N ϵ 2), Lys82 (C γ , C δ , C ϵ , N ζ), Lys85 (C δ , C ϵ , N ζ), Lys123 (C γ , C δ , C ϵ , N ζ), Gln128 (C γ , C δ , O ϵ 1, N ϵ 2), Lys176 (C γ , C δ , C ϵ , N ζ), Pro183 (C β , C γ , C δ), Lys185 (C γ , C δ , C ϵ , N ζ), Arg207 (C γ , C δ , N ϵ , C ζ , N η 1, N η 2), Lys305 (C γ , C δ , C ϵ , N ζ), Lys306 (C γ , C δ , C ϵ , N ζ), Lys319 (C β , C γ , C δ , C ϵ , N ζ), Arg345 (C γ , C δ , N ϵ , C ζ , N η 1, N η 2), Glu412 (C γ , C δ , O ϵ 1, O ϵ 2), Lys413 (C β , C γ , C δ , C ϵ , N ζ), Arg415 (C γ , C δ , N ϵ , C ζ , N η 1, N η 2), Lys439 (C δ , C ϵ , N ζ), Lys446 (C γ , C δ , C ϵ , N ζ)

Chain B: Gln81 (C γ , C δ , O ϵ 1, N ϵ 2), Asn87 (C γ , O δ 1, N δ 2), Arg153 (C γ , C δ , N ϵ , C ζ , N η 1, N η 2), His154 (C γ , N δ 1, C δ 2, C ϵ 1, N ϵ 2), Lys185 (C γ , C δ , C ϵ , N ζ), Gln199 (C γ , C δ , O ϵ 1, N ϵ 2), Arg207 (C γ , C δ , N ϵ , C ζ , N η 1, N η 2), Asp271 (C γ , O δ 1, O δ 2), Arg301 (N ϵ , C ζ , N η 1, N η 2), Arg345 (C γ , N ϵ , C ζ , N η 1, N η 2), Asp394 (C γ , O δ 1, O δ 2), Lys397 (C γ , C δ , C ϵ , N ζ), Glu412 (C γ , C δ , O ϵ 1, O ϵ 2), Lys413 (C γ , C δ , C ϵ , N ζ), Thr414 (O γ 1, O γ 2), Arg415 (C γ , C δ , N ϵ , C ζ , N η 1, N η 2), Lys416 (C γ , C δ , C ϵ , N ζ), Gln454 (C γ , C δ , O ϵ 1, N ϵ 2)

Ac-C92A–Cu–tyrosine (PDB code: 6JU9)

Missing residues

Chain A, Gly(-3)–Gly0, Ala32–Gly33, His156–Gln160, Glu308–Pro318, Gln454–Lys457

Chain B, Gly(-3)–Pro(-2), His154–Gly161, Asp304–Gly315, Glu412–Lys413, Arg455–Lys457

Missing atoms

Chain A: Ser1 (O γ), Lys10 (C γ , C δ , C ϵ , N ζ), Pro12(C γ , C δ), Lys13 (C γ , C δ , C ϵ , N ζ), Ser31 (O γ), Ser34 (C β , O γ), Asn35 (C β , C γ , O δ 1, N δ 2), Gln81 (C γ , C δ , O ϵ 1, N ϵ 2), Lys82 (C γ , C δ , C ϵ , N ζ), Lys123 (C γ , C δ , C ϵ , N ζ), Gln128 (C γ , C δ , O ϵ 1, N ϵ 2), Asn129 (C γ , O δ 1, N δ 2), Asp133 (C γ , O δ 1, O δ 2), Lys176 (C γ , C δ , C ϵ , N ζ), Gln182 (C γ , C δ , O ϵ 1, N ϵ 2), Pro183 (C β , C γ , C δ), Lys185 (C γ , C δ , C ϵ , N ζ), Arg207 (C γ , C δ , N ϵ , C ζ , N η 1, N η 2), Asp271 (C γ , O δ 1, O δ 2), Asp303 (C γ , O δ 1, O δ 2), Asp304 (C γ , O δ 1, O δ 2), Lys305 (C γ , C δ , C ϵ , N ζ), Lys306 (C γ , C δ , C ϵ , N ζ), Lys319 (C β , C γ , C δ , C ϵ , N ζ), Arg345 (C γ , C δ , N ϵ , C ζ , N η 1, N η 2), Glu412 (C γ , C δ , O ϵ 1, O ϵ 2), Lys413 (C β , C γ , C δ , C ϵ , N ζ), Arg415 (C γ , C δ , N ϵ , C ζ , N η 1, N η 2), Ser449 (O γ)

Chain B: Lys10 (C δ , C ϵ , N ζ), Gln81 (C γ , C δ , O ϵ 1, N ϵ 2), Lys82 (C γ , C δ , C ϵ , N ζ), Asp83 (C β , C γ , O δ 1, O δ 2), Ser84 (O γ), Lys85 (C β , C γ , C δ , C ϵ , N ζ), Lys123 (C γ , C δ , C ϵ , N ζ), Gln124 (C δ , O ϵ 1, N ϵ 2), Arg153 (C β , C γ , C δ , N ϵ , C ζ , N η 1, N η 2), Gln182 (C δ , O ϵ 1, N ϵ 2), Lys185 (C γ , C δ , C ϵ , N ζ), Leu187(C γ , C δ 1, C δ 2), Gln199 (C γ , C δ , O ϵ 1, N ϵ 2), Arg207 (C γ , C δ , N ϵ , C ζ , N η 1, N η 2), Trp221 (C γ , C δ 1, C δ 2, N ϵ 1, C ϵ 2, C ϵ 3, C ζ 2, C ζ 3, C η 2), Asp271 (C γ , O δ 1, O δ 2), Arg301 (C γ , C δ , N ϵ , C ζ , N η 1, N η 2), Gln316 (C γ , C δ , O ϵ 1, N ϵ 2), Arg345 (C γ , C δ , N ϵ , C ζ , N η 1, N η 2), His346 (C γ , N δ 1, C δ 2, C ϵ 1, N ϵ 2), Thr414 (O γ 1, O γ 2), Arg415 (C γ , C δ , N ϵ , C ζ , N η 1, N η 2), Lys416 (C γ , C δ , C ϵ , N ζ), Ser442 (O γ), Arg445 (C γ , C δ , N ϵ , C ζ , N η 1, N η 2), Gln454 (C γ , C δ , O ϵ 1, N ϵ 2)

Pro-C92A (PDB code: 6JUA)

Missing residues

Chain A: Gly(-3)–Gly(-1), Gly79–Pro88, His154–Gly161, Pro183–Lys185, Ser213–Phe223, Asp304–Gln316, Gln454–Glu465, Ser516–Gln527, Glu584–Asp598

Chain B: Gly(-3)–Pro(-2), Ser31–Asn35, Arg153–Gly161, Gln214–Trp221, Asp303–Gln316, Ser516–Gly532, Asp589–Asp597

Missing atoms

Chain A: Ser1 (O γ), Lys13 (C δ , C ϵ , N ζ), Ser34 (O γ), Glu73 (C γ , C δ , O ϵ 1, O ϵ 2), Thr89 (C β , O γ 1, O γ 2), Gln128 (C γ , C δ , O ϵ 1, N ϵ 2), Arg153 (C γ , C δ , N ϵ , C ζ , N η 1, N η 2), Asp162 (C γ , O δ 1, O δ 2), Gln182 (C γ , C δ , O ϵ 1, N ϵ 2), Glu206 (C γ , C δ , O ϵ 1, O ϵ 2), Arg207 (C γ , C δ , N ϵ , C ζ , N η 1, N η 2), Thr212 (O γ 1, O γ 2), Asp224 (C γ , O δ 1, O δ 2), Lys229 (C δ , C ϵ , N ζ), Asp271 (C γ , O δ 1, O δ 2), Asp274 (C β , C γ , O δ 1, O δ 2), Asp303 (C γ , O δ 1, O δ 2), Pro318 (C γ , C δ), Lys319 (C γ , C δ , C ϵ , N ζ), Arg345 (C γ , C δ , N ϵ , C ζ , N η 1, N η 2), Asp347 (C γ , O δ 1, O δ 2), Asp394 (C γ , O δ 1, O δ 2), Lys395 (C δ , C ϵ , N ζ), Glu412 (C γ , C δ , O ϵ 1, O ϵ 2), Lys413 (C β , C γ , C δ , C ϵ , N ζ), Thr414 (C β , O γ 1, O γ 2), Arg415 (C β , C γ , C δ , N ϵ , C ζ , N η 1, N η 2), Lys416 (C γ , C δ , C ϵ , N ζ), Asp440 (C γ , O δ 1, O δ 2), Ser442 (O γ), Arg443 (C γ , C δ , N ϵ , C ζ , N η 1, N η 2), Arg445 (C γ , C δ , N ϵ , C ζ , N η 1, N η 2), Ser449 (O γ), Glu466 (C γ , C δ , O ϵ 1, O ϵ 2), Lys496 (C δ , C ϵ , N ζ), Gln528 (C γ , C δ , O ϵ 1, N ϵ 2), Glu531 (C γ , C δ , O ϵ 1, O ϵ 2), Arg542 (N ϵ , C ζ , N η 1, N η 2), His546 (C γ , N δ 1, C δ 2, C ϵ 1, N ϵ 2), Lys553 (C γ , C δ , C ϵ , N ζ), Arg560 (C γ , C δ , N ϵ , C ζ , N η 1, N η 2), Glu573 (C γ , C δ , O ϵ 1, O ϵ 2), Lys575 (C γ , C δ , C ϵ , N ζ), Glu577 (C γ , C δ , O ϵ 1, O ϵ 2), Arg600 (C γ , C δ , N ϵ , C ζ , N η 1, N η 2), Arg601 (C γ , C δ , N ϵ , C ζ , N η 1, N η 2), Lys606 (C γ , C δ , C ϵ , N ζ), Asp612 (C γ , O δ 1, O δ 2), Arg615 (C γ , C δ , N ϵ , C ζ , N η 1, N η 2)

Chain B: Ser1 (O γ), Lys10 (C γ , C δ , C ϵ , N ζ), Lys13 (C γ , C δ , C ϵ , N ζ), Gln81 (C γ , C δ , O ϵ 1, N ϵ 2), Lys82 (C γ , C δ , C ϵ , N ζ), Ser84 (O γ), Lys85 (C γ , C δ , C ϵ , N ζ), Asn87 (C γ , O δ 1, N δ 2), Lys123 (C δ , C ϵ , N ζ), Gln128 (C γ , C δ , O ϵ 1, N ϵ 2), Lys131 (C γ , C δ , C ϵ , N ζ), Asp162 (C β , C γ , O δ 1, O δ 2), Lys176 (C δ , C ϵ , N ζ), Pro183 (C γ , C δ), Lys185 (C γ , C δ , C ϵ , N ζ), Leu187 (C γ , C δ 1, C δ 2), Glu206 (C γ , C δ , O ϵ 1, O ϵ 2), Arg207 (C γ , C δ , N ϵ , C ζ , N η 1, N η 2), Thr212 (O γ 1, O γ 2), Ser213 (C β , O γ), Ser222 (O γ), Phe223 (C γ , C δ 1, C δ 2, C ϵ 1, C ϵ 2, C ζ), Pro318 (C γ , C δ), Lys319 (C γ , C δ , C ϵ , N ζ), Arg345 (C γ , C δ , N ϵ , C ζ , N η 1, N η 2), Lys397 (C γ , C δ , C ϵ , N ζ), Val398 (C γ 1, C γ 2), Glu412 (C γ , C δ , O ϵ 1, O ϵ 2), Lys413 (C γ , C δ , C ϵ , N ζ), Arg415 (C γ , C δ , N ϵ , C ζ , N η 1, N η 2), Lys416 (C γ , C δ , C ϵ , N ζ), Arg443 (C γ , C δ , N ϵ , C ζ , N η 1, N η 2), Lys446 (C γ , C δ , C ϵ , N ζ), Gln454 (C γ , C δ , O ϵ 1, N ϵ 2), Lys461 (C γ , C δ , C ϵ , N ζ), Glu465 (C γ , C δ , O ϵ 1, O ϵ 2), Glu466 (C γ , C δ , O ϵ 1, O ϵ 2), Lys482 (C γ , C δ , C ϵ , N ζ), Val533 (C γ 1, C γ 2), Lys550 (C γ , C δ , C ϵ , N ζ), Lys553 (C γ , C δ , C ϵ , N ζ), Glu555 (C γ , C δ , O ϵ 1, O ϵ 2), Glu584 (C γ , C δ , O ϵ 1, O ϵ 2), Arg600 (C γ , C δ , N ϵ , C ζ , N η 1, N η 2), Lys606 (C γ , C δ , C ϵ , N ζ)

Pro-C92A (damaged) (PDB code: 6JUB)

Missing residues

Chain A: Gly(-3)-Gly0, Ala32-Gly33, Gly79-Pro88, His154-Gly161, Ser181-Lys185, Ser213-Phe223, Asp304-Gln316, Gln454-Glu465, Ser516-Gln527, Glu584-Asp598

Chain B: Gly(-3)-Gly0, Thr30-Asn35, Arg153-Gly161, Ser213-Trp221, Asp303-Gln316, Asp440-Ala441, Gly464, Ser516-Gly532, Gly585-Asp598

Missing atoms

Chain A: Ser1 (O γ), Lys13 (C γ , C δ , C ϵ , N ζ), Ser31 (O γ), Ser34 (O γ), Asn35 (C γ , O δ 1, N δ 2), Glu73 (C γ , C δ , O ϵ 1, O ϵ 2), Thr89 (C β , O γ 1, O γ 2), Lys123 (C γ , C δ , C ϵ , N ζ), Arg153 (C γ , C δ , N ϵ , C ζ , N η 1, N η 2), Asp162 (C γ , O δ 1, O δ 2), Gln199 (C γ , C δ , O ϵ 1, N ϵ 2), Glu206 (C γ , C δ , O ϵ 1, O ϵ 2), Arg207 (C γ , C δ , N ϵ , C ζ , N η 1, N η 2), Thr212 (O γ 1, O γ 2), Asp224 (C γ , O δ 1, O δ 2), Lys229 (C γ , C δ , C ϵ , N ζ), Glu240 (C γ , C δ , O ϵ 1, O ϵ 2), Asn241 (C γ , O δ 1, N δ 2), Leu270 (C β , C γ , C δ 1, C δ 2), Asp271 (C γ , O δ 1, O δ 2), Asp274 (C β , C γ , O δ 1, O δ 2), Asp303 (C γ , O δ 1, O δ 2), Pro318 (C γ , C δ), Lys319 (C γ , C δ , C ϵ , N ζ), Arg345 (C γ , C δ , N ϵ , C ζ , N η 1, N η 2), Asp347 (C γ , O δ 1, O δ 2), Asn392 (C γ , O δ 1, N δ 2), Asp394 (C γ , O δ 1, O δ 2), Lys395 (C γ , C δ , C ϵ , N ζ), Lys397 (C γ , C δ , C ϵ , N ζ), Val398 (C γ 1, C γ 2), Lys400 (C δ , C ϵ , N ζ), Phe410 (C γ , C δ 1, C δ 2, C ϵ 1, C ϵ 2, C ζ), Glu412 (C γ , C δ , O ϵ 1, O ϵ 2), Lys413 (C β , C γ , C δ , C ϵ , N ζ), Thr414 (C β , O γ 1, O γ 2), Arg415 (C β , C γ , C δ , N ϵ , C ζ , N η 1, N η 2), Lys416 (C γ , C δ , C ϵ , N ζ), Arg421 (C γ , C δ , N ϵ , C ζ , N η 1, N η 2), Asp440 (C γ , O δ 1, O δ 2), Ser442 (O γ), Arg443 (C γ , C δ , N ϵ , C ζ , N η 1, N η 2), Arg445 (C γ , C δ , N ϵ , C ζ , N η 1, N η 2), Lys446 (C γ , C δ , C ϵ , N ζ), Glu447 (C γ , C δ , O ϵ 1, O ϵ 2), Ser449 (O γ), Glu466 (C γ , C δ , O ϵ 1, O ϵ 2), Lys496 (C γ , C δ , C ϵ , N ζ), Gln528 (C γ , C δ , O ϵ 1, N ϵ 2), Glu529 (C γ , C δ , O ϵ 1, O ϵ 2), Glu531 (C γ , C δ , O ϵ 1, O ϵ 2), Arg542 (N ϵ , C ζ , N η 1, N η 2), His546 (C γ , N δ 1, C δ 2, C ϵ 1, N ϵ 2), Lys549 (C γ , C δ , C ϵ , N ζ), Lys550 (C γ , C δ , C ϵ , N ζ), Gln551 (C γ , C δ , O ϵ 1, N ϵ 2), Lys553 (C γ , C δ , C ϵ , N ζ), Arg560 (C γ , C δ , N ϵ , C ζ , N η 1, N η 2), Glu573 (C γ , C δ , O ϵ 1, O ϵ 2), Lys575 (C γ , C δ , C ϵ , N ζ), Glu577 (C γ , C δ , O ϵ 1, O ϵ 2), Arg600 (C γ , C δ , N ϵ , C ζ , N η 1, N η 2), Arg601 (C γ , C δ , N ϵ , C ζ , N η 1, N η 2), Asp604 (C γ , O δ 1, O δ 2), Lys606 (C γ , C δ , C ϵ , N ζ), Glu609 (C γ , C δ , O ϵ 1, O ϵ 2), Asp612 (C γ , O δ 1, O δ 2), Arg615 (C γ , C δ , N ϵ , C ζ , N η 1, N η 2)

Chain B: Ser1 (O γ), Lys10 (C γ , C δ , C ϵ , N ζ), Asp11 (C γ , O δ 1, O δ 2), Pro12 (C β , C γ , C δ), Lys13 (C γ , C δ , C ϵ , N ζ), His14 (C β , C γ , N δ 1, C δ 2, C ϵ 1, N ϵ 2), Glu28 (C γ , C δ , O ϵ 1, O ϵ 2), Arg36 (C γ , C δ , N ϵ , C ζ , N η 1, N η 2), Gln81 (C β , C γ , C δ , O ϵ 1, N ϵ 2), Lys82 (C β , C γ , C δ , C ϵ , N ζ), Ser84 (C β , O γ), Lys85 (C γ , C δ , C ϵ , N ζ), Asn87 (C γ , O δ 1, N δ 2), Pro88 (C γ , C δ), Lys123 (C γ , C δ , C ϵ , N ζ), Gln128 (C γ , C δ , O ϵ 1, N ϵ 2), Asn129 (C γ , O δ 1, N δ 2), Lys131 (C γ , C δ , C ϵ , N ζ), Asp133 (C γ , O δ 1, O δ 2), Lys138 (C γ , C δ , C ϵ , N ζ), Asp162 (C β , C γ , O δ 1, O δ 2), Lys176 (C γ , C δ , C ϵ , N ζ), Pro183 (C γ , C δ), Lys185 (C γ , C δ , C ϵ , N ζ), Gln186 (C γ , C δ , O ϵ 1, N ϵ 2), Leu187 (C γ , C δ 1, C δ 2), Gln199 (C γ , C δ , O ϵ 1, N ϵ 2), Glu206 (C γ , C δ , O ϵ 1, O ϵ 2), Arg207 (C γ , C δ , N ϵ , C ζ , N η 1, N η 2), Thr212 (O γ 1, O γ 2), Ser222 (O γ), Phe223 (C γ , C δ 1, C δ 2, C ϵ 1, C ϵ 2, C ζ), Asn241 (C γ , O δ 1, N δ 2), Pro318 (C γ , C δ), Lys319 (C γ , C δ , C ϵ , N ζ), Arg345 (C γ , C δ , N ϵ , C ζ , N η 1, N η 2), Asp347 (C γ , O δ 1, O δ 2), Lys395 (C γ , C δ , C ϵ , N ζ), Lys397 (C γ , C δ , C ϵ , N ζ), Val398 (C γ 1, C γ 2), Arg405 (C γ , C δ , N ϵ , C ζ , N η 1, N η 2), Glu412 (C γ , C δ , O ϵ 1, O ϵ 2), Lys413 (C γ , C δ , C ϵ , N ζ), Arg415 (C γ , C δ , N ϵ , C ζ , N η 1, N η 2), Lys416 (C γ , C δ , C ϵ , N ζ), Lys439 (C γ , C δ , C ϵ , N ζ), Ser442 (C β , O γ), Arg443 (C β , C γ , C δ , N ϵ , C ζ , N η 1, N η 2), Arg445 (C γ , C δ , N ϵ , C ζ , N η 1, N η 2), Lys446 (C γ , C δ , C ϵ , N ζ), Glu447 (C γ , C δ , O ϵ 1, O ϵ 2), Ser449 (O γ), Gln454 (C γ , C δ , O ϵ 1, N ϵ 2), Arg455 (N ϵ , C ζ , N η 1, N η 2), Lys457 (C γ , C δ , C ϵ , N ζ), Glu458 (C γ , C δ , O ϵ 1, O ϵ 2), Lys461 (C γ , C δ , C ϵ , N ζ), Asp462 (C γ , O δ 1, O δ 2), Phe463 (C γ , C δ 1, C δ 2, C ϵ 1, C ϵ 2, C ζ), Glu465 (C γ , C δ , O ϵ 1, O ϵ 2), Glu466 (C γ , C δ , O ϵ 1, O ϵ 2), Lys482 (C γ , C δ , C ϵ , N ζ), Asp492 (C γ , O δ 1, O δ 2), Lys496 (C γ , C δ , C ϵ , N ζ), Val533 (C γ 1, C γ 2), Arg542 (C γ , C δ , N ϵ , C ζ , N η 1, N η 2), Lys550 (C γ , C δ , C ϵ , N ζ), Gln551 (C γ , C δ , O ϵ 1, N ϵ 2), Lys553 (C γ , C δ , C ϵ , N ζ), Glu555 (C γ , C δ , O ϵ 1, O ϵ 2), Arg560 (N ϵ , C ζ , N η 1, N η 2), Glu573 (C γ , C δ , O ϵ 1, O ϵ 2), Lys575 (C δ , C ϵ , N ζ), Lys582 (C δ , C ϵ , N ζ), Glu584 (C γ , C δ , O ϵ 1, O ϵ 2), Arg600 (C γ , C δ , N ϵ , C ζ , N η 1, N η 2), Lys606 (C γ , C δ , C ϵ , N ζ), Glu609 (C γ , C δ , O ϵ 1, O ϵ 2), Asp612 (C γ , O δ 1, O δ 2), Arg615 (N ϵ , C ζ , N η 1, N η 2)

Pro-C92A/H103F (PDB code: 6JUC)

Missing residues

Chain A: Gly(-3)–Gly0, Gly80–Pro88, His154–Gly161, Ser213–Phe223, Lys305–Gln316, Gln454–Glu465, Ser516–Cys525, Glu584–Asp597

Chain B: Thr30–Asn35, Lys82–Asn87, His154–Gly161, Ser213–Asp224, Asp304–Gln316, Ala441–Ser443, Gly515–Gly532, Ala590–Asp597

Missing atoms

Chain A: Ser1 (O γ), Lys13 (C γ , C δ , C ϵ , N ζ), Ser34 (O γ), Thr89 (O γ 1, O γ 2), Lys123 (C γ , C δ , C ϵ , N ζ), Gln128 (C γ , C δ , O ϵ 1, N ϵ 2), Arg153 (C γ , C δ , N ϵ , C ζ , N η 1, N η 2), Asp162 (C γ , O δ 1, O δ 2), Lys176 (C γ , C δ , C ϵ , N ζ), Gln182 (C γ , C δ , O ϵ 1, N ϵ 2), Lys185 (C β , C γ , C δ , C ϵ , N ζ), Glu206 (C γ , C δ , O ϵ 1, O ϵ 2), Arg207 (C γ , C δ , N ϵ , C ζ , N η 1, N η 2), Thr212 (O γ 1, O γ 2), Asp224 (C β , C γ , O δ 1, O δ 2), Lys229 (C δ , C ϵ , N ζ), Asp271 (C γ , O δ 1, O δ 2), Asp274 (C γ , O δ 1, O δ 2), Asp303 (C γ , O δ 1, O δ 2), Asp304 (C γ , O δ 1, O δ 2), Pro318 (C β , C γ , C δ), Lys319 (C γ , C δ , C ϵ , N ζ), Arg345 (C γ , C δ , N ϵ , C ζ , N η 1, N η 2), Asp347 (C γ , O δ 1, O δ 2), Asn392 (C γ , O δ 1, N δ 2), Asp394 (C γ , O δ 1, O δ 2), Lys397 (C γ , C δ , C ϵ , N ζ), Val398 (C γ 1, C γ 2), Lys413 (C β , C γ , C δ , C ϵ , N ζ), Thr414 (O γ 1, O γ 2), Arg415 (C β , C γ , C δ , N ϵ , C ζ , N η 1, N η 2), Lys416 (C γ , C δ , C ϵ , N ζ), Asp440 (C β , C γ , O δ 1, O δ 2), Ser442 (O γ), Arg443 (C β , C γ , C δ , N ϵ , C ζ , N η 1, N η 2), Arg445 (C ζ , N η 1, N η 2), Lys446 (C γ , C δ , C ϵ , N ζ), Ser449 (O γ), Glu466 (C γ , C δ , O ϵ 1, O ϵ 2), Gln527 (C β , C γ , C δ , O ϵ 1, N ϵ 2), Gln528 (C γ , C δ , O ϵ 1, N ϵ 2), Arg542 (N ϵ , C ζ , N η 1, N η 2), Lys550 (C γ , C δ , C ϵ , N ζ), Lys553 (C γ , C δ , C ϵ , N ζ), Arg560 (C γ , C δ , N ϵ , C ζ , N η 1, N η 2), Asp598 (C γ , O δ 1, O δ 2), Arg600 (C γ , C δ , N ϵ , C ζ , N η 1, N η 2), Arg601 (N ϵ , C ζ , N η 1, N η 2), Lys606 (C γ , C δ , C ϵ , N ζ), Arg607 (C γ , C δ , N ϵ , C ζ , N η 1, N η 2), Glu609 (C γ , C δ , O ϵ 1, O ϵ 2), Arg615 (C γ , C δ , N ϵ , C ζ , N η 1, N η 2)

Chain B: Ser1 (O γ), Lys10 (C γ , C δ , C ϵ , N ζ), Lys13 (C γ , C δ , C ϵ , N ζ), Glu28 (C γ , C δ , O ϵ 1, O ϵ 2), Gln81 (C γ , C δ , O ϵ 1, N ϵ 2), Thr89 (O γ 1, O γ 2), Gln128 (C δ , O ϵ 1, N ϵ 2), Asp129 (C γ , O δ 1, O δ 2), Arg153 (C γ , C δ , N ϵ , C ζ , N η 1, N η 2), Asp162 (C γ , O δ 1, O δ 2), Lys176 (C γ , C δ , C ϵ , N ζ), Gln182 (C γ , C δ , O ϵ 1, N ϵ 2), Lys185 (C γ , C δ , C ϵ , N ζ), Leu187 (C γ , C δ 1, C δ 2), Glu206 (C γ , C δ , O ϵ 1, O ϵ 2), Arg207 (C γ , C δ , N ϵ , C ζ , N η 1, N η 2), Thr212 (C β , O γ 1, O γ 2), Asn241 (C γ , O δ 1, N δ 2), Asp303 (C γ , O δ 1, O δ 2), Pro318 (C γ , C δ), Lys319 (C γ , C δ , C ϵ , N ζ), Arg345 (C γ , N ϵ , C ζ , N η 1, N η 2), Ser387 (O γ), Lys395 (C γ , C δ , C ϵ , N ζ), Lys397 (C γ , C δ , C ϵ , N ζ), Val398 (C γ 1, C γ 2), Glu412 (C β , C γ , C δ , O ϵ 1, O ϵ 2), Lys413 (C γ , C δ , C ϵ , N ζ), Arg415 (C γ , C δ , N ϵ , C ζ , N η 1, N η 2), Lys416 (C γ , C δ , C ϵ , N ζ), Asp440 (C γ , O δ 1, O δ 2), Arg445 (C γ , C δ , N ϵ , C ζ , N η 1, N η 2), Lys446 (C γ , C δ , C ϵ , N ζ), Gln454 (C γ , C δ , O ϵ 1, N ϵ 2), Lys461 (C γ , C δ , C ϵ , N ζ), Glu465 (C γ , C δ , O ϵ 1, O ϵ 2), Arg476 (C γ , C δ , N ϵ , C ζ , N η 1, N η 2), Tyr477 (C γ , C δ 1, C δ 2, C ϵ 1, C ϵ 2, C ζ , O η), Lys482 (C γ , C δ , C ϵ , N ζ), Val533 (C γ 1, C γ 2), Lys553 (C γ , C δ , C ϵ , N ζ), Glu555 (C γ , C δ , O ϵ 1, O ϵ 2), Lys582 (C ϵ , N ζ), Glu584 (C δ , O ϵ 1, O ϵ 2), Arg600 (C γ , C δ , N ϵ , C ζ , N η 1, N η 2), Lys606 (C γ , C δ , C ϵ , N ζ), Asp612 (C β , C γ , O δ 1, O δ 2)

Pro-C92A/H103F (damaged) (PDB code: 6JUD)

Missing residues

Chain A: Gly(-3)–Gly0, Ala32-Asn35, Gly80–Pro88, His154-Gly161, Ser213-Phe223, Asp271-Trp273, Asp305-Gln316, Gln454-Glu465, Ser516-Cys525, Glu584-Asp597

Chain B: Thr30-Asn35, Lys82-Asn87, His154-Gly161, Ser213-Trp221, Asp304-Gln316, Ala441-Ser442, Gly515-Gly532, Ala590-Ser596

Missing atoms

Chain A: Ser1 (O γ), Lys13 (C γ , C δ , C ϵ , N ζ), Thr89 (O γ 1, O γ 2), Lys123 (C γ , C δ , C ϵ , N ζ), Gln128 (C γ , C δ , O ϵ 1, N ϵ 2), Asp133 (C γ , O δ 1, O δ 2), Arg153 (C γ , C δ , N ϵ , C ζ , N η 1, N η 2), Asp162 (C γ , O δ 1, O δ 2), Gln182 (C γ , C δ , O ϵ 1, N ϵ 2), Lys185 (C β , C γ , C δ , C ϵ , N ζ), Glu206 (C γ , C δ , O ϵ 1, O ϵ 2), Arg207 (C γ , C δ , N ϵ , C ζ , N η 1, N η 2), Thr212 (O γ 1, O γ 2), Asp224 (C β , C γ , O δ 1, O δ 2), Lys229 (C γ , C δ , C ϵ , N ζ), Asp274 (C γ , O δ 1, O δ 2), Asp303 (C γ , O δ 1, O δ 2), Asp304 (C γ , O δ 1, O δ 2), Pro318 (C β , C γ , C δ), Lys319 (C γ , C δ , C ϵ , N ζ), Arg345 (C β , C γ , C δ , N ϵ , C ζ , N η 1, N η 2), Asp347 (C γ , O δ 1, O δ 2), Asn392 (C γ , O δ 1, N δ 2), Asp394 (C γ , O δ 1, O δ 2), Lys397 (C γ , C δ , C ϵ , N ζ), Val398 (C γ 1, C γ 2), Glu412 (C γ , C δ , O ϵ 1, O ϵ 2), Lys413 (C β , C γ , C δ , C ϵ , N ζ), Thr414 (O γ 1, O γ 2), Arg415 (C β , C γ , C δ , N ϵ , C ζ , N η 1, N η 2), Lys416 (C γ , C δ , C ϵ , N ζ), Asp440 (C β , C γ , O δ 1, O δ 2), Arg443 (C β , C γ , C δ , N ϵ , C ζ , N η 1, N η 2), Arg445 (C ζ , N η 1, N η 2), Lys446 (C γ , C δ , C ϵ , N ζ), Ser449 (O γ), Glu466 (C γ , C δ , O ϵ 1, O ϵ 2), Gln527 (C β , C γ , C δ , O ϵ 1, N ϵ 2), Gln528 (C γ , C δ , O ϵ 1, N ϵ 2), Glu531 (C γ , C δ , O ϵ 1, O ϵ 2), Arg542 (N ϵ , C ζ , N η 1, N η 2), Lys550 (C γ , C δ , C ϵ , N ζ), Lys553 (C γ , C δ , C ϵ , N ζ), Arg560 (C γ , C δ , N ϵ , C ζ , N η 1, N η 2), Lys575 (C γ , C δ , C ϵ , N ζ), Asp598 (C γ , O δ 1, O δ 2), Arg600 (C γ , C δ , N ϵ , C ζ , N η 1, N η 2), Arg601 (C δ , N ϵ , C ζ , N η 1, N η 2), Lys606 (C γ , C δ , C ϵ , N ζ), Arg607 (C γ , C δ , N ϵ , C ζ , N η 1, N η 2), Glu609 (C γ , C δ , O ϵ 1, O ϵ 2), Asp612 (C γ , O δ 1, O δ 2), Arg615 (C γ , C δ , N ϵ , C ζ , N η 1, N η 2)

Chain B: Ser1 (O γ), Lys10 (C γ , C δ , C ϵ , N ζ), Lys13 (C γ , C δ , C ϵ , N ζ), Gln81 (C γ , C δ , O ϵ 1, N ϵ 2), Thr89 (O γ 1, O γ 2), Gln128 (C δ , O ϵ 1, N ϵ 2), Asn129 (C γ , O δ 1, N δ 2), Lys131 (C γ , C δ , C ϵ , N ζ), Arg153 (C γ , C δ , N ϵ , C ζ , N η 1, N η 2), Asp162 (C γ , O δ 1, O δ 2), Lys176 (C γ , C δ , C ϵ , N ζ), Gln182 (C γ , C δ , O ϵ 1, N ϵ 2), Lys185 (C γ , C δ , C ϵ , N ζ), Leu187 (C γ , C δ 1, C δ 2), Gln199 (C γ , C δ , O ϵ 1, N ϵ 2), Glu206 (C γ , C δ , O ϵ 1, O ϵ 2), Arg207 (C γ , C δ , N ϵ , C ζ , N η 1, N η 2), Thr212 (C β , O γ 1, O γ 2), Ser222 (O γ), Asn241 (C γ , O δ 1, N δ 2), Asp271 (C γ , O δ 1, O δ 2), Asp303 (C γ , O δ 1, O δ 2), Pro318 (C γ , C δ), Arg345 (C γ , C δ , N ϵ , C ζ , N η 1, N η 2), Asp347 (C γ , O δ 1, O δ 2), Ser387 (O γ), Lys395 (C γ , C δ , C ϵ , N ζ), Lys397 (C γ , C δ , C ϵ , N ζ), Val398 (C γ 1, C γ 2), Glu412 (C β , C γ , C δ , O ϵ 1, O ϵ 2), Lys413 (C γ , C δ , C ϵ , N ζ), Arg415 (C γ , C δ , N ϵ , C ζ , N η 1, N η 2), Lys416 (C γ , C δ , C ϵ , N ζ), Asp440 (C γ , O δ 1, O δ 2), Arg443 (C γ , C δ , N ϵ , C ζ , N η 1, N η 2), Arg445 (C γ , C δ , N ϵ , C ζ , N η 1, N η 2), Lys446 (C γ , C δ , C ϵ , N ζ), Gln454 (C γ , C δ , O ϵ 1, N ϵ 2), Lys457 (C γ , C δ , C ϵ , N ζ), Glu458 (C γ , C δ , O ϵ 1, O ϵ 2), Lys461 (C γ , C δ , C ϵ , N ζ), Glu465 (C γ , C δ , O ϵ 1, O ϵ 2), Glu466 (C γ , C δ , O ϵ 1, O ϵ 2), Arg476 (C γ , C δ , N ϵ , C ζ , N η 1, N η 2), Tyr477 (C γ , C δ 1, C δ 2, C ϵ 1, C ϵ 2, C ζ , O η), Lys482 (C γ , C δ , C ϵ , N ζ), Val533 (C γ 1, C γ 2), Lys553 (C γ , C δ , C ϵ , N ζ), Glu555 (C γ , C δ , O ϵ 1, O ϵ 2), Glu573 (C γ , C δ , O ϵ 1, O ϵ 2), Lys575 (C γ , C δ , C ϵ , N ζ), Lys582 (C γ , C δ , C ϵ , N ζ), Glu584 (C γ , C δ , O ϵ 1, O ϵ 2), Asp597 (C γ , O δ 1, O δ 2), Arg600 (C γ , C δ , N ϵ , C ζ , N η 1, N η 2), Lys606 (C γ , C δ , C ϵ , N ζ), Asp612 (C β , C γ , O δ 1, O δ 2)

Supplementary Table 3 | Interatomic distances and bond angles in the crystal structures

Pro-F513Y (Chain A) (PDB code: 6JU4)				
Cu–Cu distances*				
	CuA1	CuA2	CuB1	
CuA2	1.80 (0.04)			
CuB1	4.43 (0.02)	3.93 (0.04)		
CuB2	3.80 (0.02)	3.20 (0.04)	1.03 (0.01)	
Bond Lengths*				
	CuA1	CuA2	CuB1	CuB2
O2	2.50 (0.06)	1.76 (0.06)	2.24 (0.06)	1.73 (0.05)
His67(Nε)	2.01 (0.03)	2.26 (0.04)	-	-
His94(Nε)	2.08 (0.04)	2.13 (0.05)	-	-
His103(Nε)	2.07 (0.03)	-	-	-
Tyr513(Oζ)	-	2.93 (0.27)	-	-
DOPA513(Oζ)	-	3.03 (0.12)	-	-
DOPA513(Oε)	-	2.14 (0.06)	-	2.93 (0.07)
His328(Nε)	-	-	2.35 (0.03)	1.82 (0.03)
His332(Nε)	-	-	1.88 (0.03)	2.28 (0.03)
His372(Nε)	-	-	1.86 (0.03)	2.25 (0.03)
Angles*				
–CuA1–	His67(Nε)	His94(Nε)	His103(Nε)	
His94(Nε)	105.2 (1.4)			
His103(Nε)	130.8 (1.4)	116.7 (1.4)		
O2	79.1 (1.6)	106.2 (1.8)	110.6 (1.5)	
–CuA2–	His67(Nε)	His94(Nε)	O2	DOPA513(Oζ)
His94(Nε)	95.8 (1.9)			
O2	91.3 (2.2)	141.4 (3.1)		
Tyr513(Oζ)	101.5 (5.5)	140.7 (5.1)	73.5 (4.5)	
DOPA513(Oζ)	102.1 (2.5)	144.7 (2.7)	68.9 (2.7)	
DOPA513(Oε)	161.3 (2.6)	100.8 (2.1)	81.3 (2.9)	59.2 (2.70)
–CuB1–	His328(Nε)	His332(Nε)	His372(Nε)	O2
His332(Nε)	90.1 (1.2)			
His372(Nε)	96.0 (1.2)	161.8 (1.5)		
O2	95.5 (1.6)	102.3 (1.7)	94.2 (1.7)	
DOPA513(Oε)	64.0 (1.0)	77.4 (1.3)	120.7 (1.4)	40.6 (1.6)
–CuB2–	His328(Nε)	His332(Nε)	His372(Nε)	O2
His332(Nε)	94.0 (1.1)			
His372(Nε)	101.0 (1.2)	109.4 (1.2)		
O2	146.4 (2.1)	105.8 (2.0)	97.7 (1.9)	
DOPA513(Oε)	91.6 (1.3)	94.9 (1.5)	151.2 (1.4)	60.4 (2.1)

Pro-F513Y (Chain B) (PDB code: 6JU4)				
Cu–Cu distances*				
	CuA1	CuA2	CuB1	
CuA2	1.83 (0.04)			
CuB1	4.27 (0.02)	3.91 (0.03)		
CuB2	3.71 (0.02)	3.24 (0.03)	0.97 (0.02)	
Bond Lengths*				
	CuA1	CuA2	CuB1	CuB2
O2	2.42 (0.05)	1.73 (0.05)	2.22 (0.05)	1.73 (0.05)
His67(Nε)	2.00 (0.03)	2.24 (0.05)	-	-
His94(Nε)	2.14 (0.03)	2.13 (0.05)	-	-
His103(Nε)	2.07 (0.03)	-	-	-
Tyr513(Oζ)	-	2.97 (0.16)	-	-
DOPA513(Oζ)	-	2.96 (0.13)	-	-
DOPA513(Oε)	-	2.30 (0.07)	3.85 (0.06)	3.00 (0.06)
His328(Nε)	-	-	2.30 (0.03)	1.83 (0.03)
His332(Nε)	-	-	1.86 (0.03)	2.25 (0.03)
His372(Nε)	-	-	1.84 (0.03)	2.28 (0.03)
Angles*				
–CuA1–	His67(Nε)	His94(Nε)	His103(Nε)	
His94(Nε)	103.4 (1.4)			
His103(Nε)	130.2 (1.5)	115.4 (1.3)		
O2	82.3 (1.5)	104.0 (1.5)	114.9 (1.4)	
–CuA2–	His67(Nε)	His94(Nε)	O2	DOPA513(Oζ)
His94(Nε)	95.8 (1.9)			
O2	93.8 (2.0)	136.5 (2.8)		
Tyr513(Oζ)	105.9 (3.3)	142.0 (3.5)	73.6 (3.0)	
DOPA513(Oζ)	107.9 (2.7)	145.4 (2.9)	67.9 (2.5)	
DOPA513(Oε)	168.5 (2.4)	95.3 (1.9)	80.1 (2.4)	60.7 (2.8)
–CuB1–	His328(Nε)	His332(Nε)	His372(Nε)	O2
His332(Nε)	92.3 (1.2)			
His372(Nε)	96.0 (1.4)	153.3 (1.6)		
O2	97.5 (1.5)	103.5 (1.5)	100.5 (1.6)	
DOPA513(Oε)	64.6 (1.1)	80.1 (1.3)	126.2 (1.6)	41.5 (1.4)
–CuB2–	His328(Nε)	His332(Nε)	His372(Nε)	O2
His332(Nε)	94.8 (1.1)			
His372(Nε)	97.1 (1.3)	105.5 (1.2)		
O2	145.7 (1.9)	107.0 (1.7)	102.0 (1.7)	
DOPA513(Oε)	90.8 (1.4)	97.5 (1.4)	154.9 (1.5)	60.9 (1.8)

*Distances and angles are given in Å and degrees (°), estimated errors are given in parentheses.

Pro-C92AF513Y (Chain A) (PDB code: 6JU5)**Cu–Cu distances***

	CuA1	CuA2	CuB1
CuA2	2.56 (0.03)		
CuB1	4.53 (0.01)	4.09 (0.02)	
CuB2	4.03 (0.02)	3.59 (0.02)	0.69 (0.01)

Bond Lengths*

	CuA1	CuA2	CuB1	CuB2
O2	2.64 (0.05)	1.86 (0.05)	2.31 (0.05)	1.84 (0.05)
His67(Nε)	2.03 (0.04)	2.52 (0.04)	-	-
His94(Nε)	2.28 (0.04)	2.24 (0.05)	-	-
His103(Nε)	1.98 (0.03)	-	-	-
Tyr513(Oζ)	-	2.26 (0.08)	-	-
DOPA513(Oζ)	-	2.67 (0.10)	-	-
DOPA513(Oε)	-	1.70 (0.06)	-	3.22 (0.06)
His328(Nε)	-	-	2.28 (0.03)	2.08 (0.03)
His332(Nε)	-	-	1.88 (0.03)	2.16 (0.03)
His372(Nε)	-	-	1.92 (0.03)	2.08 (0.03)

Angles*

–CuA1–	His67(Nε)	His94(Nε)	His103(Nε)	
His94(Nε)	100.5 (1.5)			
His103(Nε)	135.6 (1.4)	121.2 (1.3)		
O2	79.2 (1.5)	87.2 (1.5)	114.6 (1.2)	
–CuA2–	His67(Nε)	His94(Nε)	O2	DOPA513(Oζ)
His94(Nε)	88.0 (1.4)			
O2	85.4 (1.8)	111.8 (2.1)		
Tyr513(Oζ)	112.0 (3.0)	157.9 (3.1)	80.5 (3.0)	
DOPA513(Oζ)	110.5 (2.6)	158.9 (2.7)	80.8 (2.4)	
DOPA513(Oε)	162.1 (2.4)	92.5 (2.5)	77.9 (2.6)	73.1 (3.2)
–CuB1–	His328(Nε)	His332(Nε)	His372(Nε)	O2
His332(Nε)	95.6(1.0)			
His372(Nε)	95.3 (1.0)	161.2 (1.2)		
O2	90.6 (1.3)	98.7 (1.4)	96.3 (1.4)	
DOPA513(Oε)	68.1 (1.0)	77.4 (1.3)	121.0 (1.3)	33.2 (1.5)
–CuB2–	His328(Nε)	His332(Nε)	His372(Nε)	O2
His332(Nε)	98.7 (1.0)			
His372(Nε)	102.5 (1.0)	123.9 (1.1)		
O2	120.5 (1.7)	105.1 (1.6)	107.3 (1.6)	
DOPA513(Oε)	85.6 (1.2)	88.7 (1.4)	143.8 (1.4)	42.6 (1.8)

Pro-C92AF513Y (Chain B) (PDB code: 6JU5)				
Cu–Cu distances*				
	CuA1	CuA2	CuB1	
CuA2	2.56 (0.03)			
CuB1	4.51 (0.02)	4.11 (0.02)		
CuB2	4.03 (0.02)	3.61 (0.02)	0.70 (0.02)	
Bond Lengths*				
	CuA1	CuA2	CuB1	CuB2
O2	2.73 (0.04)	1.89 (0.04)	2.30 (0.04)	1.90 (0.04)
His67(N ϵ)	2.01 (0.03)	2.53 (0.04)	-	-
His94(N ϵ)	2.33 (0.04)	2.26 (0.05)	-	-
His103(N ϵ)	1.98 (0.03)	-	-	-
Tyr513(O ζ)	-	2.46 (0.14)	-	-
DOPA513(O ζ)	-	2.43 (0.10)	-	-
DOPA513(O ϵ)	-	2.07 (0.05)	-	3.46 (0.05)
His328(N ϵ)	-	-	2.32 (0.03)	1.93 (0.03)
His332(N ϵ)	-	-	1.87 (0.03)	2.14 (0.03)
His372(N ϵ)	-	-	1.89 (0.03)	2.10 (0.03)
Angles*				
–CuA1–	His67(N ϵ)	His94(N ϵ)	His103(N ϵ)	
His94(N ϵ)	101.3 (1.6)			
His103(N ϵ)	136.2 (1.4)	120.0 (1.5)		
O2	76.9 (1.4)	88.1 (1.3)	115.6 (1.2)	
–CuA2–	His67(N ϵ)	His94(N ϵ)	O2	DOPA513(O ζ)
His94(N ϵ)	89.1 (1.4)			
O2	84.2 (1.6)	116.3 (2.0)		
Tyr513(O ζ)	113.7 (3.0)	153.9 (3.3)	80.1 (2.7)	
DOPA513(O ζ)	115.8 (2.4)	154.5 (2.7)	74.0 (2.4)	
DOPA513(O ϵ)	163.0 (2.0)	82.7 (1.8)	86.2 (2.0)	74.6 (2.4)
–CuB1–	His328(N ϵ)	His332(N ϵ)	His372(N ϵ)	O2
His332(N ϵ)	96.1 (1.0)			
His372(N ϵ)	95.2 (1.1)	159.0 (1.2)		
O2	95.8 (1.2)	96.4 (1.2)	99.9 (1.3)	
DOPA513(O ϵ)	63.7 (0.9)	78.2 (1.0)	122.7 (1.1)	39.3 (1.2)
–CuB2–	His328(N ϵ)	His332(N ϵ)	His372(N ϵ)	O2
His332(N ϵ)	100.2 (1.0)			
His372(N ϵ)	101.5 (1.1)	121.4 (1.1)		
O2	127.0 (1.5)	101.2 (1.4)	107.4 (1.4)	
DOPA513(O ϵ)	80.6 (1.1)	91.2 (1.1)	145.8 (1.1)	51.1 (1.4)

*Distances and angles are given in Å and degrees (°), estimated errors are given in parentheses.

Ac-C92A-Cu (Chain A) (PDB code: 6JU8)

Cu-Cu distances*				
	CuA1	CuA2	CuB1	
CuA2	2.11 (0.02)			
CuB1	4.06 (0.01)	3.68 (0.02)		
CuB2	3.67 (0.01)	3.27 (0.02)	0.62 (0.01)	

Bond Lengths*				
	CuA1	CuA2	CuB1	CuB2
O2	1.93 (0.03)	1.67 (0.03)	2.27 (0.03)	1.89 (0.03)
O3	-	2.22 (0.04)	-	-
His67(N ϵ)	2.13 (0.02)	2.21 (0.03)	-	-
His94(N ϵ)	2.21 (0.03)	2.02 (0.04)	-	-
His103(N ϵ)	2.00 (0.02)	-	-	-
His328(N ϵ)	-	-	2.18 (0.02)	1.89 (0.02)
His332(N ϵ)	-	-	1.89 (0.02)	2.20 (0.02)
His372(N ϵ)	-	-	1.86 (0.02)	2.11 (0.02)

Angles*			
-CuA1-	His67(N ϵ)	His94(N ϵ)	His103(N ϵ)
His94(N ϵ)	100.8 (1.2)		
His103(N ϵ)	134.0 (1.0)	122.6 (1.1)	
O2	86.0 (1.2)	87.3 (1.5)	108.7 (1.1)
-CuA2-	His67(N ϵ)	His94(N ϵ)	O2
His94(N ϵ)	104.6 (1.5)		
O2	90.2 (1.4)	101.6 (1.7)	
O3	111.4 (1.3)	138.2 (1.6)	98.9 (1.6)
-CuB1-	His328(N ϵ)	His332(N ϵ)	His372(N ϵ)
His332(N ϵ)	97.7 (0.7)		
His372(N ϵ)	98.2 (0.8)	141.7 (0.8)	
O2	99.2 (1.0)	117.6 (1.0)	93.9 (1.0)
-CuB2-	His328(N ϵ)	His332(N ϵ)	His372(N ϵ)
His332(N ϵ)	97.0 (0.8)		
His372(N ϵ)	99.8 (0.8)	110.4 (0.7)	
O2	127.8 (1.2)	121.0 (1.1)	98.5 (1.11)

Ac-C92A-Cu (Chain B) (PDB code: 6JU8)**Cu-Cu distances***

	CuA1	CuA2	CuB1
CuA2	2.09 (0.03)		
CuB1	4.15 (0.01)	3.70 (0.03)	
CuB2	3.67 (0.02)	3.21 (0.03)	0.72 (0.02)

Bond Lengths*

	CuA1	CuA2	CuB1	CuB2
O2	2.01 (0.04)	1.73 (0.05)	2.27 (0.04)	1.86 (0.04)
O3	-	2.34 (0.05)	-	-
His67(N ϵ)	2.04 (0.03)	2.24 (0.03)	-	-
His94(N ϵ)	2.21 (0.05)	1.96 (0.04)	-	-
His103(N ϵ)	2.01 (0.03)	-	-	-
His328(N ϵ)	-	-	2.22 (0.03)	1.92 (0.03)
His332(N ϵ)	-	-	1.92 (0.02)	2.29 (0.02)
His372(N ϵ)	-	-	1.91 (0.03)	2.18 (0.03)

Angles*

-CuA1-	His67(N ϵ)	His94(N ϵ)	His103(N ϵ)
His94(N ϵ)	98.1 (1.6)		
His103(N ϵ)	132.9 (1.3)	125.9 (1.5)	
O2	84.8 (1.4)	92.9 (1.7)	106.4 (1.4)
-CuA2-	His67(N ϵ)	His94(N ϵ)	O2
His94(N ϵ)	99.8 (1.8)		
O2	85.9 (1.9)	112.1 (2.5)	
O3	112.9 (1.6)	139.3 (2.1)	94.4 (2.0)
-CuB1-	His328(N ϵ)	His332(N ϵ)	His372(N ϵ)
His332(N ϵ)	96.7 (0.9)		
His372(N ϵ)	99.4 (1.0)	144.3 (1.0)	
O2	103.3 (1.3)	117.2 (1.3)	89.8 (1.2)
-CuB2-	His328(N ϵ)	His332(N ϵ)	His372(N ϵ)
His332(N ϵ)	94.1 (0.9)		
His372(N ϵ)	100.4 (1.2)	109.0 (1.0)	
O2	137.4 (1.7)	118.7 (1.5)	94.0 (1.5)

*Distances and angles are given in Å and degrees (°), estimated errors are given in parentheses.

Ac-C92A-Cu-tyrosine (Chain A) (PDB code: 6JU9)				
Cu-Cu distances*				
	CuA1	CuA2	CuB1	
CuA2	2.21 (0.02)			
CuB1	4.17 (0.02)	3.84 (0.02)		
CuB2	3.69 (0.02)	3.33 (0.02)	0.55 (0.02)	
Bond Lengths*				
	CuA1	CuA2	CuB1	CuB2
O2	2.04 (0.04)	1.77 (0.04)	2.30 (0.04)	1.79 (0.04)
His67(Nε)	2.13 (0.04)	2.21 (0.04)	-	-
His94(Nε)	2.48 (0.04)	2.06 (0.05)	-	-
His103(Nε)	2.02 (0.03)	-	-	-
Tyrosine(Oζ)	-	2.01 (0.13)	-	-
DOPA(Oζ)	-	2.36 (0.09)	-	-
DOPA(Oε)	-	2.13 (0.09)	-	3.09 (0.10)
His328(Nε)	-	-	2.17 (0.03)	2.13 (0.03)
His332(Nε)	-	-	1.87 (0.03)	2.11 (0.03)
His372(Nε)	-	-	1.89 (0.03)	2.04 (0.03)
Angles*				
-CuA1-	His67(Nε)	His94(Nε)	His103(Nε)	
His94(Nε)	95.0 (1.6)			
His103(Nε)	139.0 (1.4)	123.6 (1.4)		
O2	88.6 (1.3)	82.9 (1.6)	107.9 (1.2)	
-CuA2-	His67(Nε)	His94(Nε)	O2	DOPA(Oζ)
His94(Nε)	106.1 (1.8)			
O2	93.8 (1.6)	103.4 (2.0)		
Tyrosine(Oζ)	119.0 (3.1)	128.1 (3.0)	98.3 (3.0)	
DOPA(Oζ)	107.3 (2.4)	138.9 (2.9)	97.7 (2.5)	
DOPA(Oε)	173.3 (3.0)	77.1 (3.1)	79.7 (2.9)	72.6 (3.3)
-CuB1-	His328(Nε)	His332(Nε)	His372(Nε)	O2
His332(Nε)	99.9 (1.0)			
His372(Nε)	100.6 (1.2)	148.5 (1.3)		
O2	95.7 (1.2)	111.4 (1.2)	90.0 (1.2)	
DOPA(Oε)	69.0 (1.3)	80.9 (1.9)	129.0 (1.9)	44.9 (1.8)
-CuB2-	His328(Nε)	His332(Nε)	His372(Nε)	O2
His332(Nε)	93.8 (1.0)			
His372(Nε)	97.1 (1.2)	121.1 (1.2)		
O2	115.5 (1.4)	124.5 (1.4)	101.7 (1.4)	
DOPA(Oε)	79.9 (1.5)	89.8 (2.1)	149.1 (2.2)	54.4 (2.1)

Ac-C92A–Cu–tyrosine (Chain B) (PDB code: 6JU9)				
Cu–Cu distances*				
	CuA1	CuA2	CuB1	
CuA2	2.29 (0.03)			
CuB1	4.24 (0.02)	3.82 (0.03)		
CuB2	3.81 (0.02)	3.35 (0.03)	0.61 (0.02)	
Bond Lengths*				
	CuA1	CuA2	CuB1	CuB2
O2	2.14 (0.05)	1.80 (0.05)	2.26 (0.05)	1.81 (0.05)
His67(Nε)	2.12 (0.04)	2.36 (0.05)	-	-
His94(Nε)	2.37 (0.05)	2.11 (0.06)	-	-
His103(Nε)	1.99 (0.04)	-	-	-
Tyrosine(Oζ)	-	2.19 (0.06)	-	-
His328(Nε)	-	-	2.22 (0.03)	1.98 (0.03)
His332(Nε)	-	-	1.91 (0.03)	2.16 (0.03)
His372(Nε)	-	-	1.89 (0.03)	2.11 (0.04)
Angles*				
–CuA1–	His67(Nε)	His94(Nε)	His103(Nε)	
His94(Nε)	100.6 (1.9)			
His103(Nε)	139.0 (1.6)	118.3 (1.7)		
O2	88.0 (1.7)	84.8 (1.9)	107.0 (1.5)	
–CuA2–	His67(Nε)	His94(Nε)	O2	
His94(Nε)	101.0 (1.9)			
O2	89.8 (2.1)	101.9 (2.5)		
Tyrosine(Oζ)	109.2 (1.9)	142.1 (2.3)	100.6 (2.2)	
–CuB1–	His328(Nε)	His332(Nε)	His372(Nε)	
His332(Nε)	97.5 (1.2)			
His372(Nε)	101.4 (1.4)	150.9 (1.4)		
O2	94.9 (1.5)	109.6 (1.6)	90.6 (1.6)	
–CuB2–	His328(Nε)	His332(Nε)	His372(Nε)	
His332(Nε)	97.8 (1.1)			
His372(Nε)	102.2 (1.4)	118.9 (1.3)		
O2	121.5 (1.9)	118.9 (1.8)	97.7 (1.8)	

*Distances and angles are given in Å and degrees (°), estimated errors are given in parentheses.

Pro-C92A–Cu (Chain A) (PDB code: 6JUA)			
Cu–Cu distances*			
	CuA		
CuB	3.68 (0.02)		
Bond Lengths*			
	CuA	CuB	
O2	2.18 (0.05)	1.70 (0.06)	
His67(Nε)	2.02 (0.05)	-	
His94(Nε)	2.15 (0.05)	-	
His103(Nε)	2.23 (0.05)	-	
His328(Nε)	-	1.94 (0.06)	
His332(Nε)	-	2.06 (0.05)	
His372(Nε)	-	2.25 (0.05)	
Angles*			
–CuA–	His67(Nε)	His94(Nε)	His103(Nε)
His94(Nε)	102.3 (2.1)		
His103(Nε)	119.4 (2.0)	112.6 (1.8)	
O2	96.1 (2.1)	113.3 (2.0)	111.9 (1.9)
–CuB–	H328(Nε)	H332(Nε)	H372(Nε)
H332(Nε)	99.1 (1.9)		
H372(Nε)	103.2 (2.0)	119.7 (1.7)	
O2	126.5 (2.5)	113.0 (2.3)	96.8 (2.2)

Pro-C92A–Cu (Chain B) (PDB code: 6JUA)				
Cu–Cu distances*				
	CuA			
CuB	3.55 (0.01)			
Bond Lengths*				
	CuA	CuB	O1	
O1	1.92 (0.05)	1.94 (0.05)	-	
O2	2.00 (0.05)	1.88 (0.05)	1.47 (0.06)	
His67(Nε)	2.02 (0.05)	-	-	
His94(Nε)	2.13 (0.05)	-	-	
His103(Nε)	2.26 (0.05)	-	-	
His328(Nε)	-	1.93 (0.05)	-	
His332(Nε)	-	2.05 (0.04)	-	
His372(Nε)	-	2.20 (0.05)	-	
Angles*				
–CuA–	His67(Nε)	His94(Nε)	His103(Nε)	O1
His94(Nε)	101.4 (1.9)			
His103(Nε)	110.8 (1.9)	109.6 (1.7)		
O1	139.7 (2.1)	95.5 (2.2)	97.3 (1.8)	
O2	97.0 (2.0)	122.2 (2.1)	114.0 (1.9)	43.9 (1.7)
–CuB–	H328(Nε)	H332(Nε)	H372(Nε)	O1
H332(Nε)	95.1 (1.7)			
H372(Nε)	98.1 (2.0)	115.7 (1.5)		
O1	92.9 (2.0)	141.0 (1.9)	100.9 (1.8)	
O2	137.6 (2.2)	114.2 (2.0)	96.0 (2.0)	45.1 (1.8)
–O1–	CuB			
CuA	133.7 (3.0)			
–O2–	CuB			
CuA	132.4 (3.0)			

*Distances and angles are given in Å and degrees (°), estimated errors are given in parentheses.

Pro-C92AH103F–Cu (Chain A) (PDB code: 6JUC)			
Cu–Cu distances*			
	CuA		
CuB	3.77 (0.02)		
Bond Lengths*			
	CuA	CuB	
O2	1.49 (0.06)	2.29 (0.07)	
His67(Nε)	2.00 (0.06)	-	
His94(Nε)	1.98 (0.06)	-	
His328(Nε)	-	2.17 (0.05)	
His332(Nε)	-	1.96 (0.04)	
His372(Nε)	-	1.96 (0.04)	
Angles*			
–CuA–	His67(Nε)	His94(Nε)	
His94(Nε)	107.5 (2.4)		
O2	110.3 (2.9)	142.2 (3.3)	
–CuB–	H328(Nε)	H332(Nε)	H372(Nε)
H332(Nε)	99.1 (1.6)		
H372(Nε)	98.9 (1.6)	143.8 (1.8)	
O2	98.0 (2.0)	107.6 (1.9)	100.6 (1.9)

Pro-C92AH103F-Cu (Chain B) (PDB code: 6JUC)**Cu-Cu distances***

	CuA
CuB	3.48 (0.02)

Bond Lengths*

	CuA	CuB	O1
O1	1.63 (0.04)	2.26 (0.06)	-
O2	1.87 (0.05)	1.82 (0.04)	1.54 (0.06)
His67(Nε)	2.01 (0.04)	-	-
His94(Nε)	1.94 (0.05)	-	-
His328(Nε)	-	1.96 (0.04)	-
His332(Nε)	-	2.06 (0.04)	-
His372(Nε)	-	2.09 (0.04)	-

Angles*

-CuA-	His67(Nε)	His94(Nε)	O1	
His94(Nε)	105.7 (1.9)			
O1	149.2 (2.4)	103.6 (2.7)		
O2	100.4 (1.7)	153.6 (2.1)	51.4 (2.1)	
-CuB-	H328(Nε)	H332(Nε)	H372(Nε)	O1
H332(Nε)	97.7 (1.5)			
H372(Nε)	97.7 (1.5)	124.0 (1.8)		
O1	88.7 (1.9)	123.8 (1.7)	110.1 (1.8)	
O2	131.1 (2.2)	107.4 (1.7)	101.6 (1.7)	42.5 (1.6)
-O1-	CuB			
CuA	125.9 (3.0)			
-O2-	CuB			
CuA	140.1 (2.8)			

*Distances and angles are given in Å and degrees (°), estimated errors are given in parentheses.